NKS-430
ISBN 978-87-7893-520-5

Source Localization by Inverse Methods (SLIM)

Jens Havskov Sørensen[1] (co-ordinator)
Heiko Klein[2], Magnus Ulimoen[2]
Lennart Robertson[3]
Jan Pehrsson[4]
Bent Lauritzen[5]
Dan Bohr[6], Agnieszka Hac-Heimburg[6], Carsten Israelson[6]
Anna Maria Blixt Buhr[7], Jonas Lindgren[7]
Tero Karhunen[8], Tuomas Peltonen[8]

[1]Research and Development Department,
Danish Meteorological Institute (DMI)
[2]Norwegian Meteorological Institute (MET Norway)
[3]Swedish Meteorological and Hydrological Institute (SMHI)
[4]PDC-ARGOS
[5]Center for Nuclear Technologies, Technical University of Denmark
(DTU Nutech)
[6]Nuclear Division, Danish Emergency Management Agency (DEMA)
[7]Swedish Radiation Safety Authority (SSM)
[8]Radiation and Nuclear Safety Authority (STUK)

January 2020

Abstract

In early October 2017, the International Atomic Energy Agency (IAEA) was informed by Member States that low concentrations of Ru-106 were measured in high-volume air samples in Europe from routine monitoring networks. However, no information was given that an accidental release of Ru-106 had taken place. Such events signify the need for prompt and accurate responses from national radiation protection authorities in such cases. This requires that methodologies, suited for operational use, are developed for spatial and temporal localization of the source of contamination based on available monitoring data.

For operational use, nuclear decision-support systems (DSSs) should be extended with modules handling such monitoring data automatically, e.g. by employing the European Radiological Data Exchange Platform (EURDEP), and conveying selected data to the national meteorological centre accompanied by a request to run an atmospheric dispersion model in inverse mode. The aim would be to determine a geographical area in which to find the potential release point as well as the release period.

In the first year of SLIM (2019), the following results are obtained:

- Two case studies are identified and selected, viz. the European Tracer Experiment (ETEX-1) and the October 2017 case of Ru-106 in Europe.
- Methods for temporal and spatial source localization are developed, implemented and described.
- Deterministic numerical weather prediction (NWP) model data are derived from the European Centre for Medium-Range Weather Forecasts (ECMWF) corresponding to the selected cases.
- Quality-controlled measurement data of ground-level concentration are obtained from filter stations.
- The inverse methods for source localization are applied by using the DERMA, MATCH and SNAP atmospheric dispersion models to both cases.

Key words

nuclear emergency preparedness, atmospheric dispersion model, source localization, concentration measurements

NKS-430
ISBN 978-87-7893-520-5
Electronic report, January 2020

NKS Secretariat
P.O. Box 49
DK - 4000 Roskilde, Denmark
Phone +45 4677 4041
www.nks.org
e-mail nks@nks.org

Source Localization by Inverse Methods (SLIM) – first-year report

First Year Report of the NKS-B SLIM activity

(Contract: AFT/B(19)6)

Jens Havskov Sørensen[1] (co-ordinator)

Heiko Klein[2]
Magnus Ulimoen[2]

Lennart Robertson[3]

Jan Pehrsson[4]

Bent Lauritzen[5]

Dan Bohr[6]
Agnieszka Hac-Heimburg[6]
Carsten Israelson[6]

Anna Maria Blixt Buhr[7]
Jonas Lindgren[7]

Tero Karhunen[8]
Tuomas Peltonen[8]

[1]Research and Development Department, Danish Meteorological Institute (DMI)

[2]Norwegian Meteorological Institute (MET Norway)

[3]Swedish Meteorological and Hydrological Institute (SMHI)

[4]PDC-ARGOS

[5]Center for Nuclear Technologies, Technical University of Denmark (DTU Nutech)

[6]Nuclear Division, Danish Emergency Management Agency (DEMA)

[7]Swedish Radiation Safety Authority (SSM)

[8]Radiation and Nuclear Safety Authority (STUK)

Table of contents

Introduction 4
Atmospheric Dispersion Models 5
The Danish Emergency Response Model of the Atmosphere (DERMA) 5
The Multi-scale Atmospheric Transport and Chemistry model (MATCH) 5
The Severe Nuclear Accident Program (SNAP) 6
Case Studies 7
ETEX-1 7
Sampling network stations 7
Synoptic situation 8
Sampling network 10
Tracer release 10
Results of DERMA 11
Results of MATCH 15
Results of SNAP 19
The Autumn 2017 Case of Ru-106 23
Results of DERMA 24
Results of MATCH 27
Results of SNAP 30
ARGOS and Source Localization 32
Concentration Measurements in ARGOS 32
Request for Source Localization Calculation from ARGOS 33
Area of interest 34
Time period of interest 34
Types of measurements 34
Permanent gamma-monitors and filter stations 35
Presenting results from Source Localization Calculation in ARGOS 36
Conclusions and Outlook 37
References 38

Introduction

In early October 2017, the International Atomic Energy Agency (IAEA) was informed by Member States that low concentrations of Ru-106 were measured in high-volume air samples in Europe from routine monitoring networks. However, no information was given that an accidental release of Ru-106 had taken place. Such events signify the need for prompt and accurate responses from national radiation protection authorities in such cases. This requires that methodologies, which are suited for operational use, are developed for spatial and temporal localization of the source of contamination based on available monitoring data.

For operational use, nuclear decision-support systems (DSSs) should be extended with modules handling such monitoring data automatically, e.g. by employing the European Radiological Data Exchange Platform (EURDEP), and conveying such data to the national meteorological centre accompanied by a request to run an atmospheric dispersion model in inverse mode, i.e. to run the adjoint model backwards in time. The aim would be to determine a geographical area in which to find the potential release point as well as the release period.

In the first year of the SLIM project, the following results are obtained:

- Two case studies are identified and selected, viz. the ETEX-1 and the October 2017 case of Ru-106 in Europe.
- Methods for temporal and spatial source localization are developed, implemented and described.
- Deterministic numerical weather prediction (NWP) model data are derived from the European Centre for Medium-Range Weather Forecasts (ECMWF) corresponding to the selected cases.
- Quality-controlled measurement data of ground-level concentration are obtained.
- The inverse methods for source localization are applied by using the DERMA, MATCH and SNAP atmospheric dispersion models to both cases.
- Results are intercompared.

In the previous NKS-B project MUD (Sørensen *et al.*, 2014), a methodology was developed for quantitative estimation of the uncertainty of atmospheric dispersion modelling stemming from the inherent uncertainties of meteorological model predictions. Subsequently, in the projects FAUNA (Sørensen *et al.*, 2016) and MESO (Sørensen *et al.*, 2017), the implications for nuclear emergency preparedness and management were studied also for short-range models and by applying the methodology to the Fukushima Daiichi emergency. Furthermore, a methodology was developed in the AVESOME project (Sørensen *et al.*, 2019) quantifying the combined effects of uncertainties of the source-term descriptions and the meteorological data on atmospheric dispersion prediction. Means to implement the uncertainties in DSSs, and the impacts on real-time emergency management, were described.

In the anticipated continuation of the SLIM project in 2020, the inherent meteorological uncertainties will be taken into account by incorporating the MUD methodology in the inverse modelling approach aiming at localizing the source. Previously, due to lack of computational power, such methods could not be applied for operational real-time decision support. However, with modern supercomputing facilities available e.g. at national meteorological centres the proposed methodology should be feasible for real-time use, thereby adding value to decision support.

Atmospheric Dispersion Models

The Danish Emergency Response Model of the Atmosphere (DERMA)

The Danish Emergency Response Model of the Atmosphere (DERMA) (Sørensen *et al.*, 2007; Sørensen, 1998) is a comprehensive numerical regional and meso-scale atmospheric dispersion model developed at the Danish Meteorological Institute (DMI). The model is used operationally for the Danish nuclear emergency preparedness, for which the Danish Emergency Management Agency (DEMA) is responsible (Hoe *et al.*, 2002). Besides, the model is employed for veterinary emergency preparedness (Sørensen *et al.*, 2000; 2001; Mikkelsen *et al.*, 2003; Gloster *et al.*, 2010a; 2010b), where it is used for assessment of airborne spread of animal diseases, e.g. foot-and-mouth disease. DERMA may also be used to simulate atmospheric dispersion of chemical substances, biological warfare agents and ashes from volcanic eruptions, and it has been employed for probabilistic nuclear risk assessment (Lauritzen *et al.*, 2006; 2007; Baklanov *et al.*, 2003; Mahura *et al.*, 2003; 2005).

The main objective of DERMA is to predict the dispersion of a radioactive plume and the accompanied deposition. However, the model may also be used in situations where an increased level of radioactivity has been measured but no information is received on radioactive releases. In such cases, inverse (adjoint) modelling may be applied whereby potential sources of radioactivity may be localised and release rates estimated.

The three-dimensional model is of Lagrangian type making use of a hybrid stochastic particle-puff diffusion description, and it is currently capable of describing plumes at downwind distances up to the global scale (Sørensen *et al.*, 1998). The model utilizes aerosol size dependent dry and wet deposition parameterisations as described by Baklanov and Sørensen (2001).

Currently, DERMA makes use of analysed and forecasted meteorological data of various deterministic versions at DMI of the NWP model Harmonie (Bengtsson *et al.*, 2017) covering North-western Europe, Greenland and the Faeroes, and from the global model developed and operated by the European Centre for Medium-range Weather Forecasts (ECMWF). Further, DERMA utilizes the COMEPS ensemble prediction system, which is based on the Harmonie model.

DERMA is interfaced with the Accident Reporting and Guidance Operational System (ARGOS) (Hoe *et al.*, 1999; 2002), a PC based nuclear decision-support system developed by the Prolog Development Center (PDC). The integration of DERMA with the ARGOS system is effectuated through automated online digital communication and exchange of data between the ARGOS system and the DMI High Performance Computing (HPC) facility.

The Multi-scale Atmospheric Transport and Chemistry model (MATCH)

The Multi-scale Atmospheric Transport and Chemistry model (MATCH) (Robertson *et al.*, 1999) is multi-purpose Eulerian chemical transport model (CTM) developed by the SMHI. The model is used for emergency application such as nuclear and natural events (volcanos), aerosol dynamics and optics (Andersson *et al.*, 2015), complex chemistry, and data assimilation (Robertson and Langner, 1998; Kahnert, 2008; Kahnert, 2018). The MATCH model is used operationally for chemical forecasts in CAMS (Copernicus Atmospheric Monitoring Service) and for SSM (Swedish Radiation Safety Authority) serving the ARGOS system needs (Hoe *et al.*, 1999; 2002). Other applications are studies for air quality and health

issues in climate projections. In most applications MATCH is used as a limited-area model on various possible scales, but also for global applications.

The MATCH model is basically an Eulerian model but for emergency applications a Lagrangian particle model is used in the near field of the emission location.

A wide range of possible driving meteorological data is applicable like analyses and forecasts from HARMONIE, IFS (ECMWF) and WRF.

The Severe Nuclear Accident Program (SNAP)

The Norwegian Meteorological Institute (MET-Norway) is responsible for modelling atmospheric dispersion of radioactive debris in the event of a nuclear emergency related to a nuclear accident or detonation. An additional task of the MET-Norway in a nuclear emergency is to identify unknown sources of radiation indicated by elevated levels of measurement. The basic tool used by the MET-Norway for such events is the Severe Nuclear Accident Program (SNAP) (Bartnicki *et al.*, 2011; Klein and Bartnicki, 2018).

The SNAP model was developed at the MET-Norway in 1994 as a Lagrangian particle model. The present version is fully operational at the MET-Norway and takes into account atmospheric transport and deposition of gases, noble gases and particles of different size and density emitted during nuclear accidents or explosions. SNAP can also be run remotely by experts from the Norwegian Radiation and Nuclear Safety Authority (DSA) where the Norwegian Crisis Committee is located.

Once released into the air, radioactive gases and particles are subject to advection, turbulent diffusion and deposition (dry and wet). In the SNAP calculations, the advection process is immediately followed by the diffusion process. A random walk approach is used to parameterise horizontal and vertical diffusion. When large and dense particles are released, gravitational settling is more effective than vertical diffusion, and this process is taken into account. The SNAP model has been used both for simulations of historical events, e.g. nuclear detonations in Novaya Zemlya, Chernobyl Accident (Bartnicki *et al.*, 2016), and real-time simulations, e.g. the Fukushima accident. It was tested in the ETEX experiment and showed good agreement with observations (Saltbones *et al.*, 1998). SNAP is the dispersion model currently used by the MET-Norway in the Center of Excellence: CERAD CoE.

Case Studies

ETEX-1

After the Chernobyl accident in April 1986 and the adoption of the Convention on Early Notification of a Nuclear Accident (IAEA, 1986), the International Nuclear Safety Advisory Group (INSAG) of the International Atomic Energy Agency (IAEA) recommended inter alia that the IAEA should, in collaboration with the World Meteorological Organisation (WMO), review and intercalibrate the models of atmospheric transport of radionuclides over short and long distances and of radionuclide deposition on terrestrial surfaces, and establish a database for validation studies on models.

Following this recommendation, the joint IAEA/WMO Atmospheric Transport Model Evaluation Study (ATMES) was initiated in November 1986. The objective of ATMES was to compare the evolution of the radioactive cloud (I-131 and Cs-137) with the evolution predicted by mathematical models for atmospheric dispersion, using as input only the estimated source term of the Chernobyl accident.

The ATMES suffered, however, from a number of weaknesses regarding lack of monitoring data and large uncertainties regarding the source term. Therefore, it was decided to carry out a tracer experiment in Europe. The sponsoring organisations were the European Commission (EC), the World Meteorological Organization (WMO) and the International Atomic Energy Agency (IAEA), and later joined by the US Department of Energy (USDOE).

The experiment was named ETEX, European Tracer Experiment (Graziani, Klug and Nodop, 1998; ETEX web-site, 2019). It was designed to test the readiness of interested services to respond in the case of an emergency, to organise the tracer release and compile a data set of measured air concentrations and to investigate the performance of long-range atmospheric transport and dispersion models using that data set. In total, thirty-six organisations around the world were involved in the project.

Sampling network stations

It was planned to start the sampling operations at each station about 6 hours before the expected time of tracer arrival to obtain a contemporaneous measurement of the tracer background levels and to ensure the arrival was not missed. Each station was designed to sample over a period of 72 consecutive hours (24 three-hour samples), with sampling starting time progressively delayed from West to East. The stations closest to the source started sampling 3 hours before the release start; the most distant stations ended sampling 90 hours after the release start.

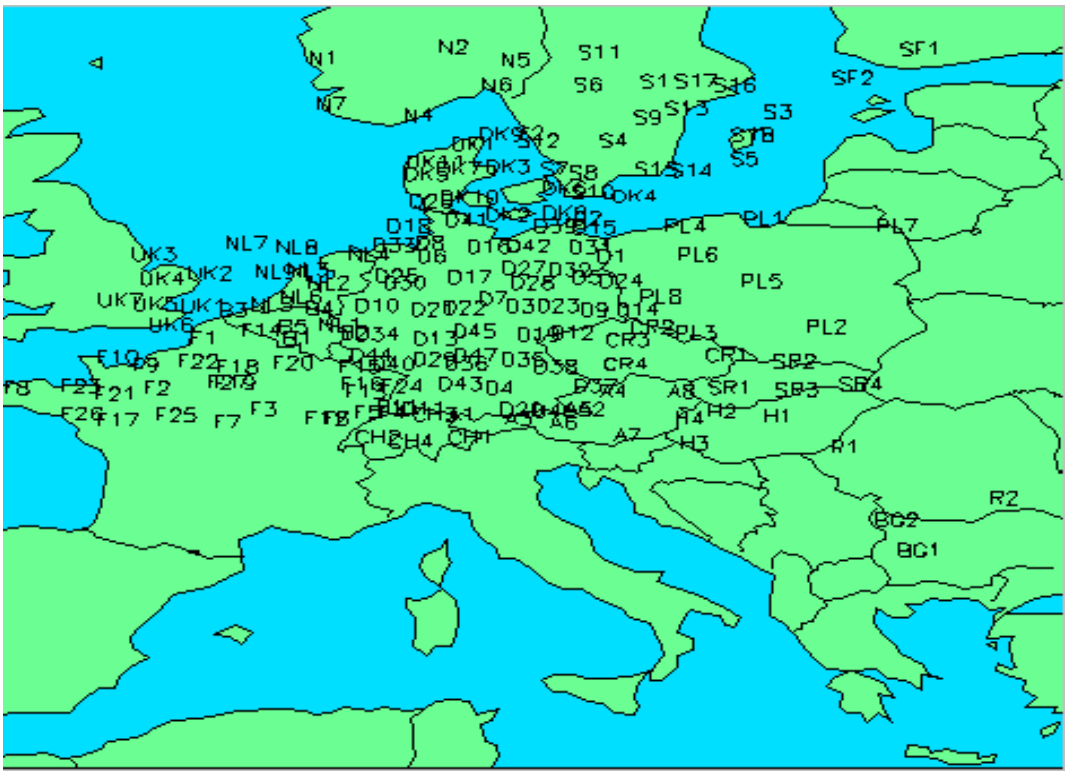

Figure 1 ETEX Sampling network (ETEX web-site, 2019).

Synoptic situation

Weather predictions suggested the following conditions on Sunday 23 October, 1994:

- the presence of a rather strong West to South-westerly flow, advecting the tracer during the experiment over several tracer stations
- no centre of high- or low-pressure, and no extending ridges or troughs, would have passed close to the release site
- no frontal systems would have passed the release site shortly before, during or after the release

Therefore, on Friday 21 October, 1994, the alert procedure was started.

The synoptic situation on 23 October, 1994

A deep low, 975 hPa, to the East of Scotland was slowly moving north, maintaining a strong south-westerly flow over the release-site (Rennes). The advected air was unstable, with showers, some accompanied by thunder and squall-lines. Similar observations could be made from satellite pictures. The 12:00 UTC radio sounding of Brest showed a temperature profile which was unstable with respect to moist air, allowing the development of shower clouds up to about 28000 ft. Also the radio sounding of Paris showed an unstable atmosphere but with lower water vapour content. At both locations, the upper winds were Southwest and rather strong. The release started at 16:00 UTC.

The synoptic situation on 24 October

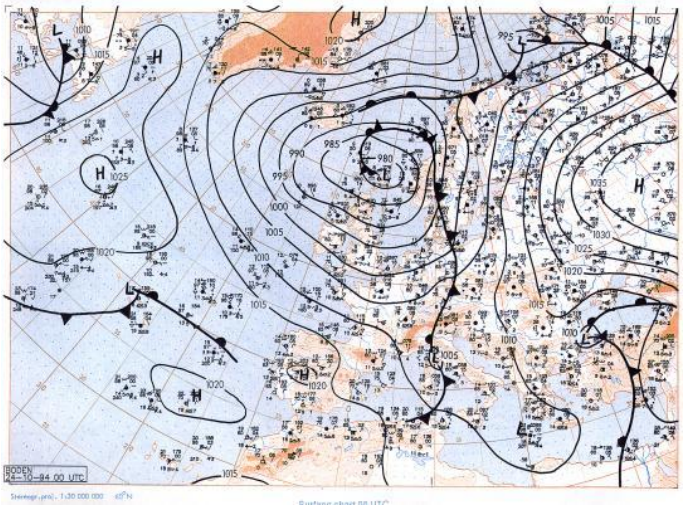

Figure 2 24 October, 1994, 00 UTC (ETEX web-site, 2019).

There was still an unstable flow over the release site and the advection area. However, because of the northerly movement of the controlling low over the North Sea, the wind in the advection area decreased. The expected cold front was to be seen south of Ireland.

The synoptic situation on 25 October, 1994

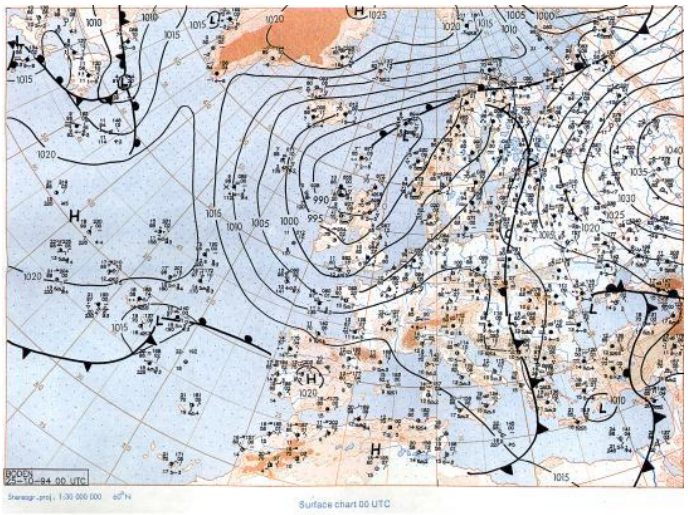

Figure 3 25 October, 1994, 00 UTC (ETEX web-site, 2019).

The further deepening of the mentioned cold front had not developed. The system was to be seen as a minor secondary low, at 52°N, 5°E. The cold front over The Netherlands, an instability front with showers, had the pressure pattern of a trough. The wind was backing more to the south with the approach of the front during the day, and after the passage of this front the wind was veering to the Southwest.

The synoptic situation on 26 October, 1994

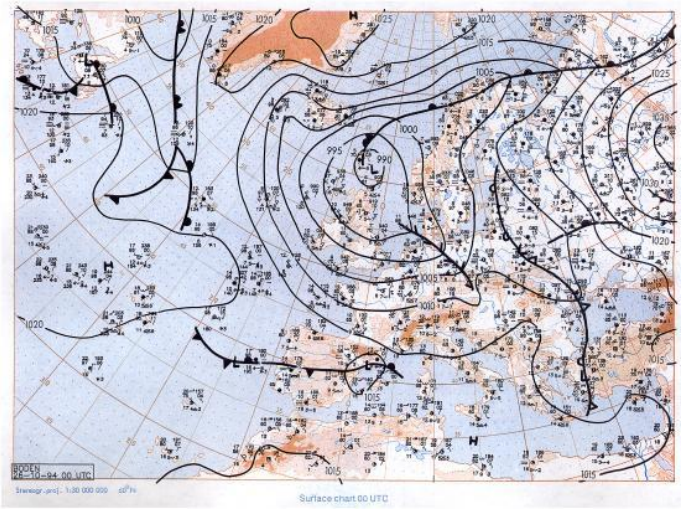

Figure 4 26 October, 1994, 00 UTC (ETEX web-site, 2019).

There was still a complex low-pressure system over the North Sea and Scotland. Shower weather with a wind tending to veer a bit over Western Europe towards west-southwest. The high-pressure cell over the Black Sea indicated that southerly winds could block any further movements of the tracer cloud towards the East.

Sampling network

The sampling network consisted of 168 ground-level sampling stations in western and eastern Europe. National meteorological services hosted the samplers at a number of WMO synoptic stations over their territory. Thus, ETEX could take advantage of this existing network, which is homogeneously distributed throughout Europe and linked to the WMO.

A final number of 168 sampling stations were selected, almost all located at existing WMO stations. Three samplers were located in the North Sea: one on a Dutch oil platform, the other two on gas platforms. The average spacing between two sampling stations in the resulting configuration was about 80 km.

Each station was labelled with one or two letters identifying the Country where it was located, and numbered sequentially.

Tracer release

Atmospheric tracers were released in the form of a homogeneous air stream containing a few percent of perfluoromethylcyclohexane (PMCH) tracer. The gas stream passed through a small chimney where the gas was released at the top.

The first release started at 16:00 UTC on October 23, 1994, and lasted 11 hours and 50 minutes. 340 kg of the non-depositing inert gas PMCH (perfluoromethylcyclohexane) were released from Monterfil (48°03’30”N, 2°00’30”W) at an average flow rate of 8.0 g/s.

Results of DERMA

Inverse atmospheric dispersion modelling

For each of the ETEX-1 filter station measurements corresponding to non-zero three-hour average tracer concentrations (in total 939 data), the DERMA model has been run in inverse mode backwards in time using a negative time step (Sørensen, 2018). Thereby the whereabouts of the released substance, PMCH, is estimated before arriving at the filter stations (Rao, 2007; Pudykiewicz, 1998); see Figure 5 for a few examples. The observed time-average concentration values are used by the dispersion model by tracing PMCH back in time from the filter stations at measurement heights with start concentration values within the averaging time periods given by the measured average values. We assume that the detected PMCH originates from the same geographically fixed ground-level release location allowing for the release to have taken place during a finite time period.

Model calculated influence functions, e.g. concentration, are shown at 2 m above ground. Obviously, the influence functions extend further in the vertical, but concentration values aloft are not shown here. As depicted in Figure 5, individual measurements do not pin-point the location of the potential release point giving rise to extended geographical sectors only. However, by identifying the overlap of the inverse plumes, one obtains a better localization. The slight inconsistencies between some of the inverse plumes may well be accounted for by the inherent meteorological uncertainties.

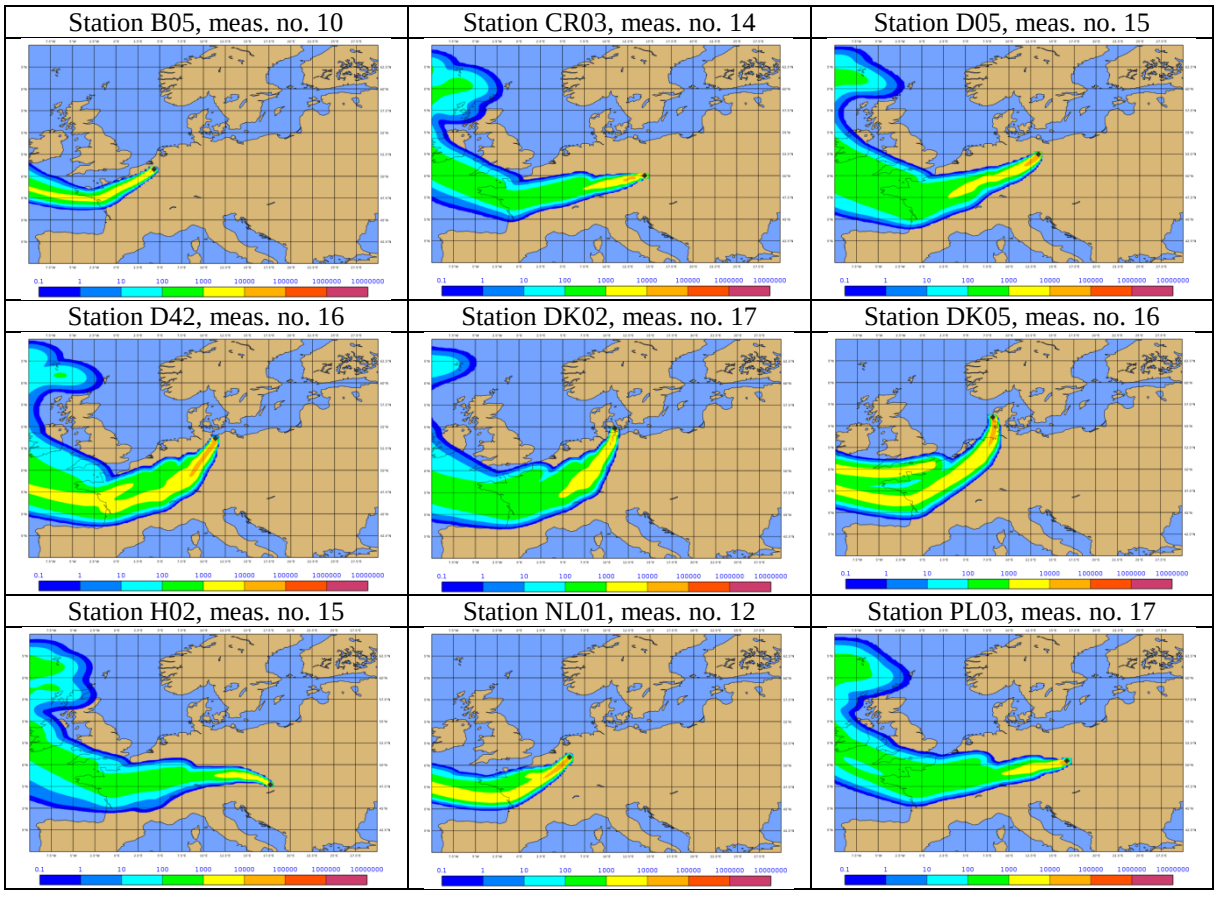

Figure 5 Time-integrated 2-m concentration in arbitrary units of inverse PMCH plumes valid at 1994-10-22, 06 UTC. The filter stations are indicated by black diamonds. For a given filter station, the measurement number (meas. no.) indicates the data point used in the 30-member time series of three-hour average concentration values measured.

In the following, both the temporal and the spatial behaviour of the inverse plumes are studied, i.e. the concentrations are correlated both in time and space. We are attempting to identify the geographic and temporal intersection of the plumes, since a release from the intersection will influence all stations having provided measurements above the detection limits. This methodology resembles the variational approach applied to the adjoint of an Eulerian model presented by Robertson and Langner (1998) and Robertson (2004). The origin of this approach is a single iteration in the variational approach where the gradient of the model error is determined by the observations. Seibert (2000, 2001, 2002) used a Lagrangian model run in backward mode to determine the source, e.g. in the context of the Comprehensive Nuclear-Test-Ban Treaty (CTBT).

Considering the ensemble of individual inverse plumes, one may apply ensemble statistical methods as employed on the results of forward dispersion calculations for a numerical weather prediction ensemble combined with a source-term ensemble describing the inherent meteorological and source-term uncertainties, cf. Sørensen *et al.* (2019). One may e.g. calculate the ensemble average of each time step involved in the time series of inverse instantaneous concentrations, cf. Figure 6. The ensemble average is not ideal for localizing the release point. However, it is useful for illustrating the mechanism of the inverse methodology.

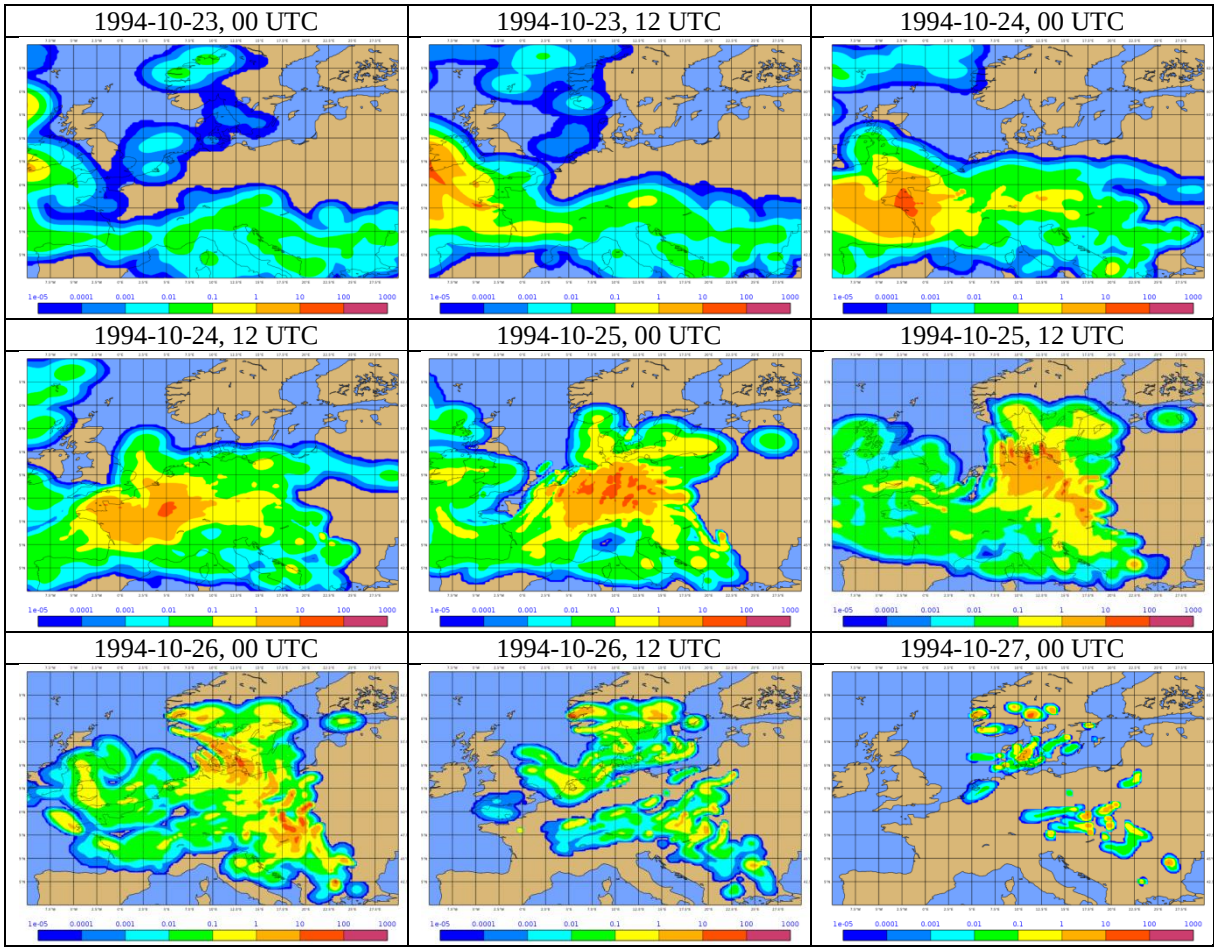

Figure 6 Time series of the set of ensemble-average inverse concentration values corresponding to the filter station measurements.

The release is assumed to have taken place from a ground-level location which can be found in the overlap of the instantaneous inverse concentration plumes. With accurate measurements representing the plume well both geographically and temporally, this overlap can be described in terms of the ensemble percentiles. It should, however, be noted that in the early phase of an accidental release where only few measurements are available, the problem is likely to be ill-conditioned.

For operational use, the best percentage value to be used for the quantile calculation is not known a priori. This value depends on how well-conditioned the problem is, i.e. how well the observations match the plume geographically and temporally, as well as on the distribution of the measured average concentration data. Thus, the recommendation is to calculate a range of percentiles, which is feasible from a computational point of view. By employing the percentile method, outliers are disregarded, and effectively a level-of-agreement approach is applied.

Low concentration values close to the detection limit or close to a potentially fluctuating background pose a difficulty due to the large relative uncertainties involved. In general, there is a risk that measurements of such values in fact do not represent the actual release but instead fluctuations in the background, or (very) low releases from elsewhere. On the other hand, there might be valuable information in such low or zero-value measurements. Imposing a threshold concentration value for the calculations aiming at localizing the point source, and thereby disregarding such difficulties, requires knowledge on detection limits for the stations involved. For the current scenario involving PMCH, the natural background value is expected to be close to zero, and in the calculations presented here, all non-zero measurement data are included.

In Figure 7 is shown the time series of the 70th percentile of the set of inverse concentration values corresponding to the filter station measurements.

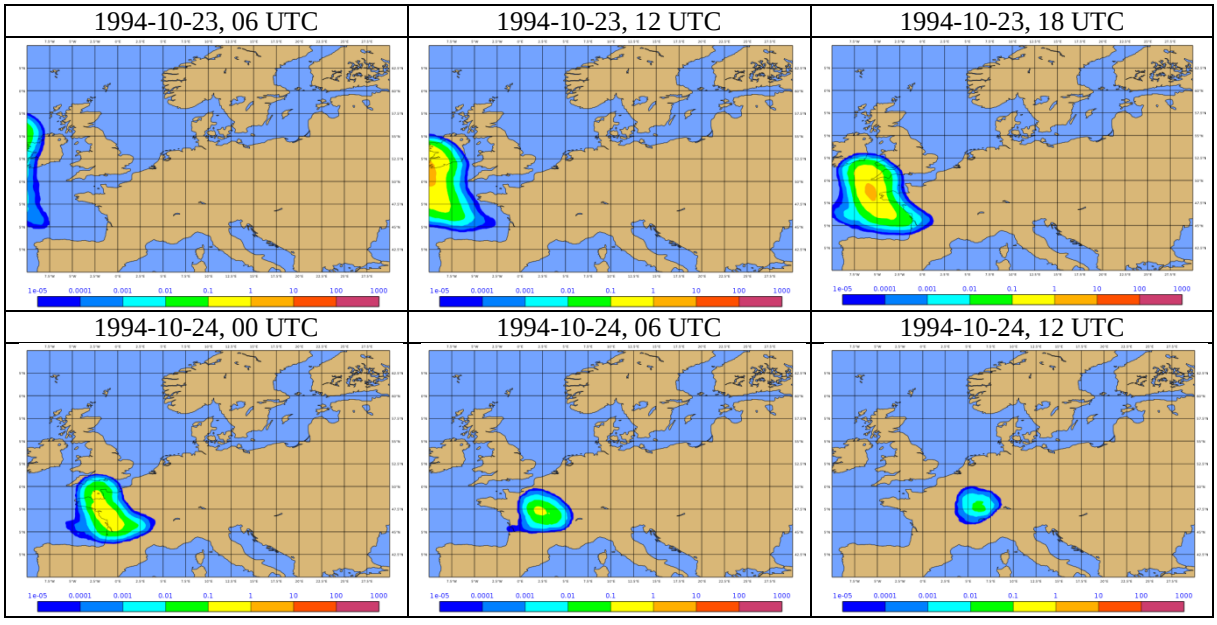

Figure 7 Time series of the 70th percentile of the set of inverse concentration values corresponding to the filter station measurements.

According to the calculated percentile maps, the release point should be found in western France in regions Brittany, Normandy or Pays de la Loire, or in the Celtic Sea. Further, the model calculations show that a release from the actual ETEX release site in Brittany near Rennes should have taken place between around 15 UTC on 23 October and 3 UTC on 24 October. The actual release started at 16 UTC on 23 October, and lasted until 4 UTC on 24 October.

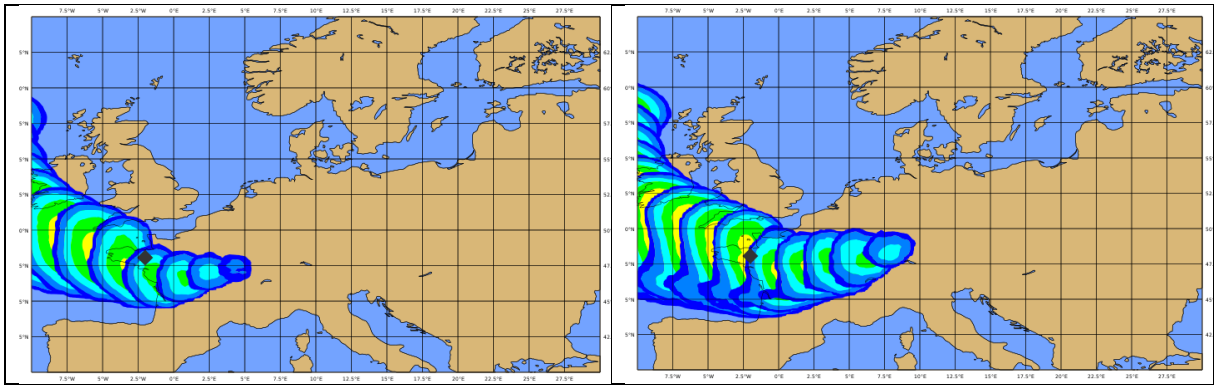

Figure 8 Estimates of the potential location of the release site. The left-hand figure consists of the overlapping time series of three-hourly 60th percentile inverse concentration maps, the right-hand figure 70th percentile maps. The maps range from 1994-10-23, 00 UTC, to 1994-10-24, 15 UTC. With a black diamond, the ETEX release point is indicated.

The time series of these 60th percentile maps has been combined in one plot in the left-hand side of Figure 8, which thereby depicts the estimate of the potential location of the release of PMCH. In the right-hand side is shown the corresponding figure using the 70th percentile maps. The larger the percentage used for the percentile, the larger the disagreement between the individual inverse concentration calculations corresponding to measured values is accepted.

From a computational point of view, the method for point source localization is very efficient on a high-performance computing (HPC) facility. This is due to the independency between the backward calculations corresponding to each of the measurement data, which implies that the scalability, i.e. the level of parallelization, is at optimum. The parallelization can either be integrated in the dispersion model employed, or be obtained by running the model natively in parallel for each measurement. The former, which is employed by DERMA, is preferable due to the reduction of the amount of input data (the three-dimensional numerical weather prediction model data), which for the latter will have to be repeated for each measurement.

Results of MATCH

The MATCH model have been run for two setups: Markov Chain Monte Carlo (MCMC) and the approach adopted for the DERMA model described above. The MCMC approach belongs to the family of Bayesian inference methods (Smith and Gelfand, 1992), where the probabilities of source locations are evaluated stepwise in order to find the most likely location (Keats *et al.*, 2006; Keats *et al.* 2008; Yee, 2008; Yee 2012).
The main differences between the two approaches are:

- MCMC is searching through the probability landscape for the most likely source location in time and space.
- The DERMA approach leads to likely source location areas at different times from the ranked overlap of individual observation contributions.
- MCMC may use all available observations.
- The DERMA may be applied to a reduced set of observations to limit the computational load.
- The both approaches could be computational demanding.
- The MCMC may not always converge to the proper source location.
- The DERMA approach is rather robust.

Markov Chain Monte Carlo

The MCMC approach is dependent on forward calculations where neither the location nor the source term is known beforehand. A way to close this is to use an adjoint simulation fed by the observed values as an indication of both the temporal and vertical profiles of the emissions. This simulation is valid over the entire grid so any location could be suggested. The amplitude of the source is then still missing. This could be retrieved by performing a test forward run followed by a bias correction against the observations. This will then scale up or down the source term used. In the end, the square difference between the model and the observations (cost function, J) is derived. Assuming Gaussian probabilities, J is also the negative exponent of a Gaussian posterior probability ($\exp(-J)$) for this location.

The process is to first select a start position for the very first source to evaluate. Here some expert judgement is needed. Having evaluated the probability for this location a random step is taken into the neighbourhood, and the process is repeated. If the new probability increases, the next step is taken from the new location. If the probability decreases, a new location is kept or discarded by the probability given by the ratio of the two probabilities (Metropolis-Hastings approach (Hastings, 1970)). A random number (0–1) will then be evaluated against the ratio probability. If the random number is less than the ratio probability, the new location is accepted for taking a new step, otherwise discarded, and a new try is made from the previous step. This will make up a trace where the underlying probability landscape is step by step revealed. If converging, the algorithm will give a trail that in the end is circulating around the location of most likely location.

Figure 9 shows a (successful) example of the MCMC search pattern. The panel to the left shows the posterior probabilities for visited locations, and to the right the mean search path of possible source locations (weighted mean by means of the probability of each location).

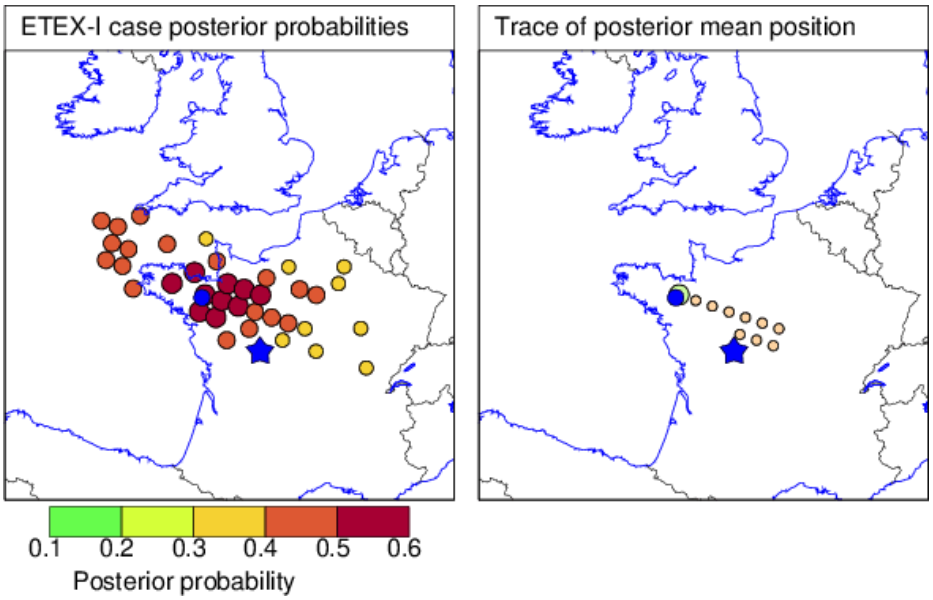

Figure 9 Successful localisation of the ETEX-I source. The posterior probabilities for visited locations are shown to the left and the mean path to the right (start at the blue star and end green circle). The true release location is marked with a blue bullet.

Figure 10 illustrates when the localisation is not fully successful, and fails in one of the showed cases.

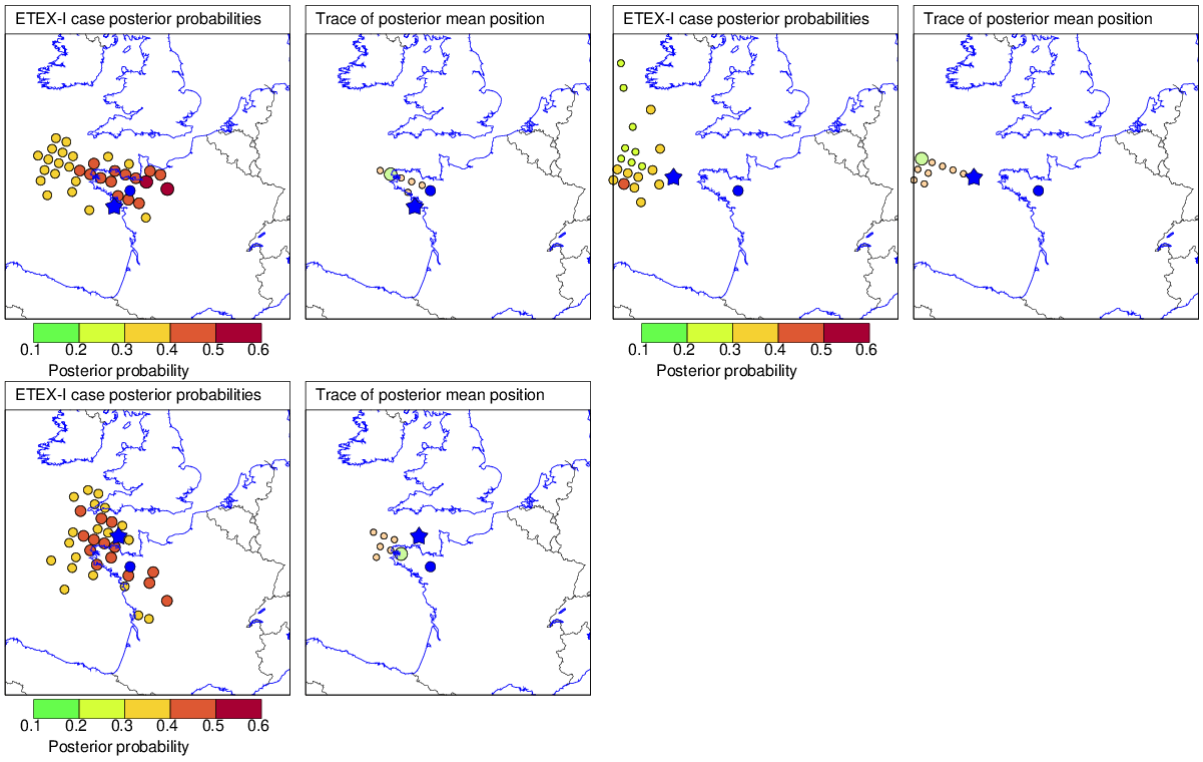

Figure 10 Example of somewhat less successful localisations of the ETEX-I release site. Posterior probabilities are shown to the left and the mean search path to the right. Start point is denoted by a blue star and the true location by a blue bullet. The upper right illustrates when the algorithm end up confused.

In conclusion the MCMC has some potential but need expert judgement in order to select the initial location for the procedure.

Percentiles of individual adjoint plumes

The DERMA percentile approach described above was also evaluated using the MATCH model. In this case a subset of 50 filter measurements were selected (in the presentation above with DERMA all measurements were used). The 10 measurements with the highest values were first selected, and then additional 40 measurements were randomly selected by weighted bootstrapping (conditional on measured values). Figure 11 shows the selected sites that are well spread over the area.

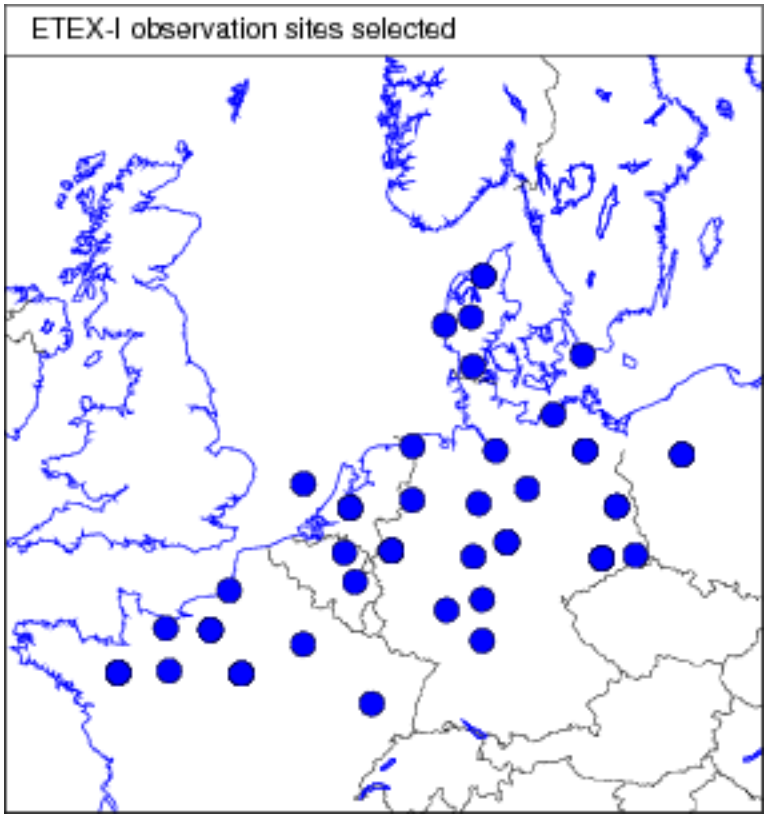

Figure 11 The locations from which 50 measurements where selected for the percentile approach. Some sites were represented with more than one filter measurement.

The individual adjoint runs were made for each measurement by assigning a unit response assumed valid over a depth of 50 m and distributed over the time-interval for the measurement (3 hours). Each such backward plume where then scaled by the measured value in a post-processing step. Figure 12 illustrates the difference between a single adjoint simulation using all ETEX filter measurements versus superimposing a set of individual adjoint plumes. As the source may have a vertical extension, the total column values are used. The essential features are present when using a reduced set of measurements for adjoint calculations. Figure 13 shows the 70^{th} percentile of inverse total columns. The percentiles are normalised to simplify equal colour legend. The major difference to results of the DERMA model (Figure 8) is that the percentiles (and release site potential) become more elongated in MATCH with longer inverse transport.

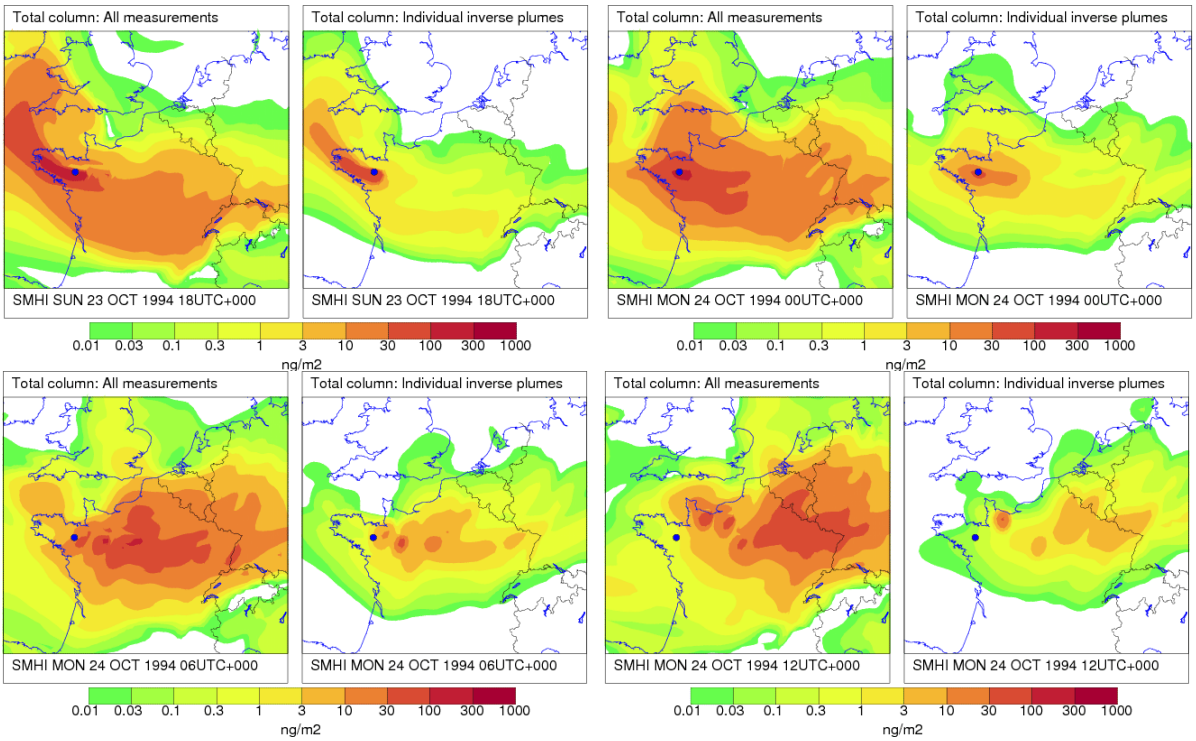

Figure 12 Illustration of the difference between adjoint backward simulations for single run using all measurements (left frame in each panel) and superimposed 50 individual adjoint runs (right frame). The total column values are plotted. The ETEX-I release site is marked with a dark bullet. The dates goes from 23 Oct 18 UTC, 1994 (top left), 24 Oct 00 UTC (top right), 24 Oct 06 UTC (bottom left) and 24 Oct 12 UTC (bottom right).

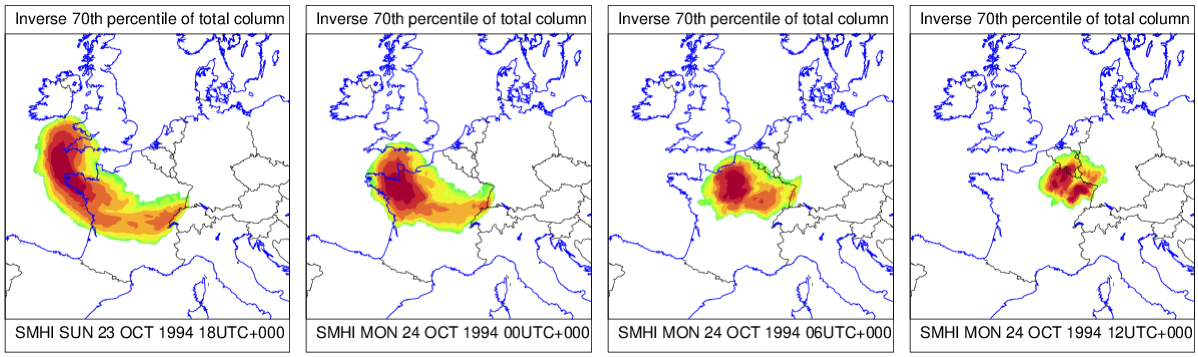

Figure 13 Assignments of possible source areas as given by 70th percentile of total column values from 50 individual inverse plumes. The percentiles are normalised to make the plots share the colour scale. The plots cover the dates 23 Oct 18 UTC to 24 Oct 12 UTC (1994) in steps of 6 hours.

Results of SNAP

A run of the atmospheric dispersion model results in a field containing the concentrations at a given point in time. We can label the field above a chosen threshold as the Field Of Regard (FOR), using the same terminology as Wotawa *et al.* (2003). Any point in the FOR, when run with the adjoint model, will encapsulate the original point in the adjoint FOR. An example of the FOR for adjoint runs is shown in Figure 14.

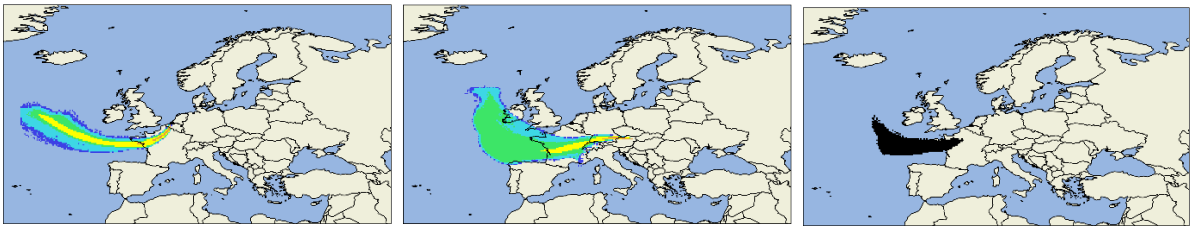

Figure 14 FOR from adjoint plumes from two measurements (acting as sources in the adjoint model) (left and middle), and intersection of FOR (right).

A single receptor will through the adjoint FOR give information on a likely area of release. Masking can be used to combine several FOR from two or more measurements. This approach is illustrated in Figure 14, with two arbitrary adjoint plumes from receptors combined (adjoint concentration exceeding a threshold/not exceeding) into a mask showing locations that are likely to have contained the release. This approach can be further extended by including measurements below the Limit Of Detection (LOD). The adjoint FOR for such a measurement does not contain the release location, or is unlikely to be above the threshold.

This gives a straight-forward method of using all measurements from all stations. Such inclusion of measurements below LOD are shown on the right in Figure 15, which combines the result of Figure 14 with the adjoint plume on the left of Figure 15. These stations and measurements were selected to illustrate this method in the optimal case.

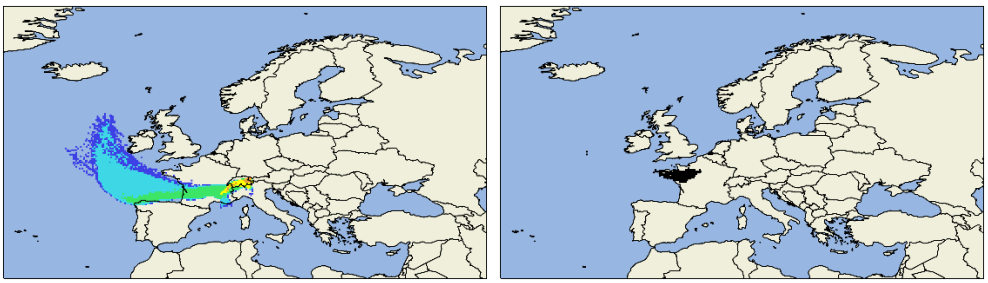

Figure 15 FOR from adjoint plume for a station which had measurement below LOD (left), intersection of Figure 14 and the left figure (right).

This approach is, however, not scalable with more measurements, as the potential area will be a decreasing set which might not converge to the true area. This is especially prominent when errors are present, either due to uncertainties in atmospheric conditions, detection limits, or inaccuracies in the models, including incompleteness of the FOR due to numerical limitations of particles in the Lagrangian model. The following contains a simplified Bayesian approach utilizing a similar methodology, retaining the ease and efficiency of the previous model.

The overlap of adjoint plumes provides information as to where the release would have the highest likelihood. We view areas with adjoint concentrations above a certain threshold as in the field-of-regard. A higher overlap of the different FOR results in a higher probability of a

release from the locations in the overlap, whilst areas not covered by the FOR have a lower probability. From a single measurement and the corresponding FOR, one can assign a probability that the threshold is exceeded. As a first approximation, we could assign the probabilities

$$\Pr\left(T_i > T \mid \mathrm{rel}_{\{x,y,\bar{t}\}}\right) = \begin{cases} p_0 & \text{if FOR from } \mathrm{rel}_{\{x,y,\bar{t}\}} \\ p_1 & \text{if not} \end{cases}$$

for threshold exceedance. Here $\mathrm{rel}_{\{x,y,\bar{t}\}}$ is a singular release scenario at (x, y) over the time $\bar{t}$ (corresponding to the sampling time), $T_i > T$ is the hypothesis of threshold exceedance given this release, and $p_0 + p_1 = 1$. p_0 should be higher than p_1 as the FOR provides more evidence, but the ratio between these probabilities does not have to be fixed. Setting $p_0 = p_1$ will not contribute any evidence, and $p_0 = 1, p_1 = 0$ is the intersection from the above section.

For stations with measurements under LOD, an analogous probability can be set by

$$\Pr\left(T_i < T \mid \mathrm{rel}_{\{x,y,\bar{t}\}}\right) = \begin{cases} p_2 & \text{if FOR from } \mathrm{rel}_{\{x,y,\bar{t}\}} \\ p_3 & \text{if not} \end{cases}$$

where the hypothesis is now that the threshold will not be exceeded given such a release. The probabilities $p_2 + p_3 = 1$, with $p_2 > p_3$. The optimal probabilities are not known a priori, but values can be adjusted a posteriori based on heuristics.

To determine how well a release would fit all the measurements (consistency), we start with the following equation, which yields the consistency requirement of the measurements.

$$\Pr\left(\text{measurements consistent with rel.} \mid \mathrm{rel}_{\{x,y,\bar{t}\}}\right) = \prod_i \Pr\left(T_i > T \mid \mathrm{rel}_{\{x,y,\bar{t}\}}\right) \prod_j \Pr\left(T_i < T \mid \mathrm{rel}_{\{x,y,\bar{t}\}}\right)$$

Where T is a threshold set by the detection limit of each station. The index i goes over all measurements above LOD, while the j indexes across all measurements below LOD. This formulation also appears in (Yee, 2017; Senocak *et al.*, 2008), but including different functionals to estimate per station probabilities. Applying Bayes' rule gives the following relation, relating the release location and duration to the consistency of the measurements:

$$\Pr\left(\mathrm{rel}_{\{x,y,\bar{t}\}} \mid \text{consistent}\right) \propto \Pr\left(\text{consistent} \mid \mathrm{rel}_{\{x,y,\bar{t}\}}\right) \Pr\left(\mathrm{rel}_{\{x,y,\bar{t}\}}\right)$$

The prior $\Pr\left(\mathrm{rel}_{\{x,y,\bar{t}\}}\right)$ is set to be uniform, as we have no knowledge regarding location of the source term before adding the signal from the measurements. Information regarding likely sources could here be added by stakeholders, to limit the search space to probable release areas such as radiological facilities.

The probabilities in the hypothesis should be determined by a relation between the adjoint concentration and source parameters. A full model should take into account LOD and sampling times for the stations, dilution volumes, and other expert knowledge, atmospheric dispersion parametrisation, and atmospheric uncertainty. For performance reasons these probabilities have been set to constants. This simplified approach still yields good results for the ETEX case. The weighting between the two hypotheses could be adjusted based on the number of samples per group, to take into account sample size bias.

The implementation takes the following form. An adjoint run with uniform unit release lasting the length of the measurement (or non-measurement) is run as far back in time as deemed necessary. The resulting fields can be iterated over windows of size 1, 2, … n hours, adding the FORs to a merged FOR, to find the dependence on release duration. The probabilities can so be estimated by collapsing the merged FORs through the probability hypotheses given above. To find the most likely locations, the fields containing the highest performing members can be presented. An overlapping time series can also be produced for a given release duration, allowing an estimate of time of release. Estimates for location can also be found by combining the largest probabilities over a certain period of time.

This method only requires building a listing of adjoint runs for each measurement, with later adaptations and adjustments of probabilities being able to run quickly on the produced ensemble of runs. All the steps above can be performed in parallel on supercomputers, allowing rapid estimates of likely source locations. Additional measurements arriving from online radioactivity measurements could be added to the ensembles, allowing renewed probabilities and adjusted location estimate.

Applied to the ETEX-1 case

The hypothesis probabilities are set to $(0.75, 0.25)$ for both hypotheses. Applying the method to the ETEX-I case using all the measurements results in fields for both a variable start time and a variable duration. Sorting these by highest occurrence of probability gives a way to determine the locations of highest probability. Figure 16 shows the areas in which the 9 highest ranked maps are displayed. These show qualitatively the same areas, and estimates the location somewhat north-east of the actual release location. The initial start time of the release is overestimated, and is from 1-4 hours after the actual start. The duration of the release is both under- and over-estimated, but within 6 hours.

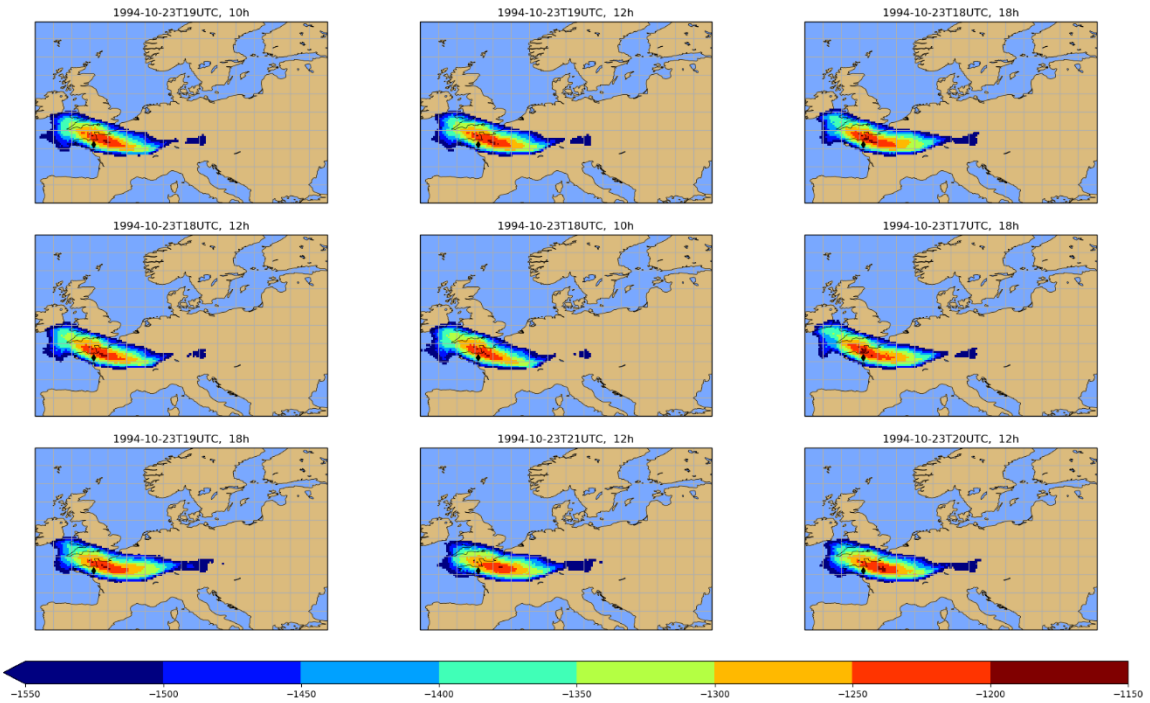

Figure 16 Nine plots showing the highest probabilities for the ETEX-1 case. Black diamond shows the known release location, with the colours showing the logarithmic probability density. The times on the top of each subfigure shows the start time of the estimate, with the duration of the release given in hours. Compare with the actual release at 1994-10-23, 16 UTC and 12 hour duration.

The overlapping time series of probabilities in Figure 17 shows how the probability density changes with time, becoming gradually more dispersed both forwards and backwards in time from the most likely starting time. The difference in maximum probability between the two subplots shows the larger duration as more probable than a shorter duration. This is further supported in Figure 18, which shows the probability density integrated in time, extracting the maximum probability along for each time step.

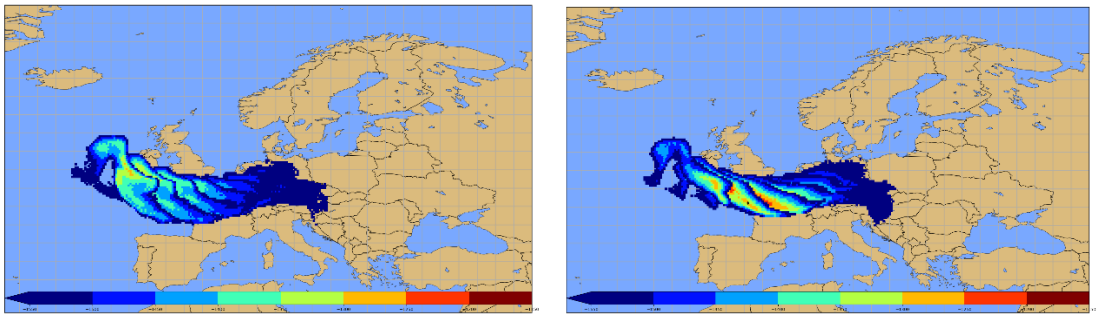

Figure 17 Time series of probability densities assuming a release lasting an hour (left) and ten hours (right). Each slice is separated in time by two hours.

This method seems to be limited by the sampling duration of the stations (three hours) which is mirrored in the start time, duration, and most probable location being roughly three hours from the actual release scenario. The meteorological uncertainties are not taken into account, which could potentially affect the method in meteorological conditions less predictable than ETEX-1.

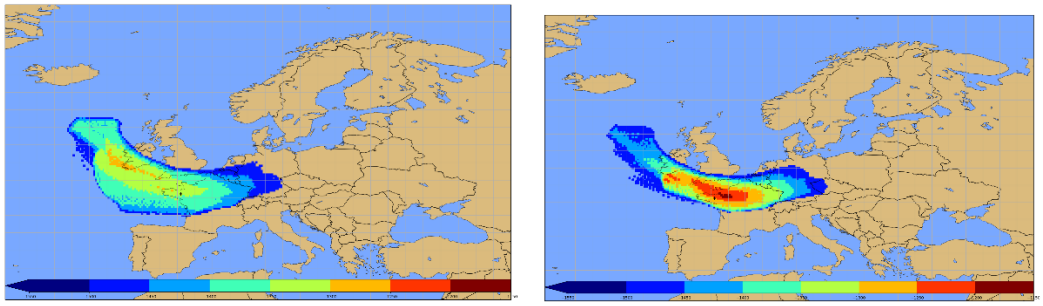

Figure 18 Maximum probability density for a release duration of one hour (left) and 10 hours (right).

The Autumn 2017 Case of Ru-106

During the period 3–6 October 2017, the Incident and Emergency Centre of the International Atomic Energy Agency (IAEA) was informed by Member States that low concentrations of Ru-106 were measured in high-volume air samples in Europe. The detected isotopes did not contain any other radionuclides (e.g. other fission products such as Cs-137) and were at levels far below those requiring public protective actions. Corresponding data and information were obtained from the IAEA (2017). The data comprise 387 measurements of Ru-106, some of which correspond to levels below minimum detectable activities. The data are time-average concentrations corresponding to varying time periods of up to seven days.

From a meteorological point of view, seven days can be a long time with potentially a number of meteorological phenomena such as front passages etc. taking placing at the release site within the period. Possible sampling scenarios include evenly distributed low concentrations at the station site throughout the sampling period, or brief high concentrations corresponding to a narrow plume passing over the site in a short while. Therefore, such measurement data should possibly be discarded in a localization study**.** The discarded data can, however, be used for verification purposes.

Results of DERMA

The filter station measurement data employed are confined to non-zero measurements and sampling periods less than 36 hours. Thereby, the data set is reduced to 89 measurement data. For each of these data, the DERMA model has been run in inverse mode backwards in time. Thereby the whereabouts of Ru-106 is estimated before arriving at the filter stations; cf. Figure 19 for a few examples. The observed time-average concentration values are used by the dispersion model by tracing Ru-106 back in time from the filter stations at measurement heights with start concentration values within the averaging time periods given by the measured average values. We assume that the detected Ru-106 originates from the same geographically fixed ground-level release location allowing for the release to have taken place during a finite time period.

As shown in Figure 19, individual measurements do not pin-point the location of the potential release point giving rise to extended geographical sectors only. However, by identifying the overlap of the inverse plumes, one obtains a better localization. In the following, model calculated influence functions, e.g. concentration, are shown at 2 m above ground. Obviously, the influence functions extend further in the vertical, but due to the assumption of a ground-level release, concentration values aloft are not shown here.

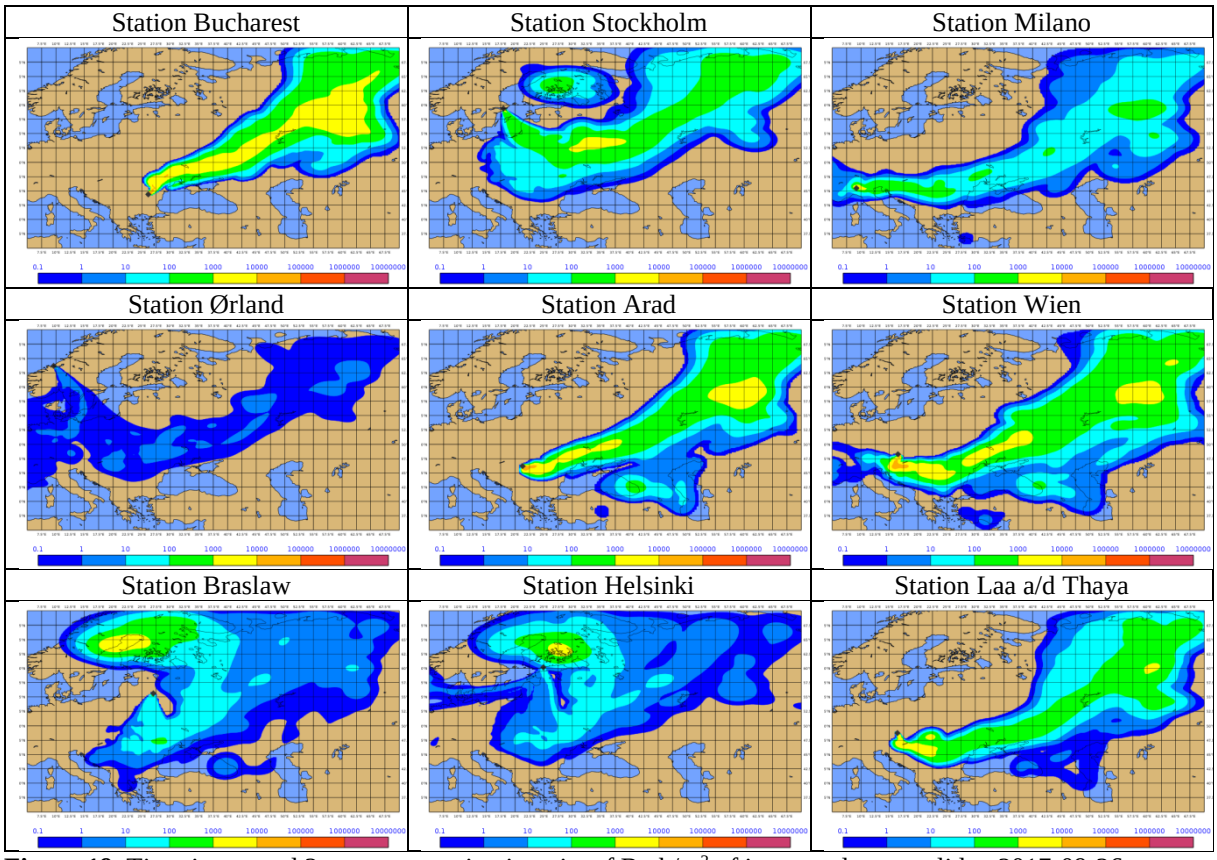

Figure 19 Time-integrated 2-m concentration in units of Bq h/m^3 of inverse plumes valid at 2017-09-26, 00 UTC. The filter stations are indicated by black diamonds.

In Figure 20 is shown the time series of the 20th percentile of the set of inverse concentration values corresponding to the non-zero filter station measurements.

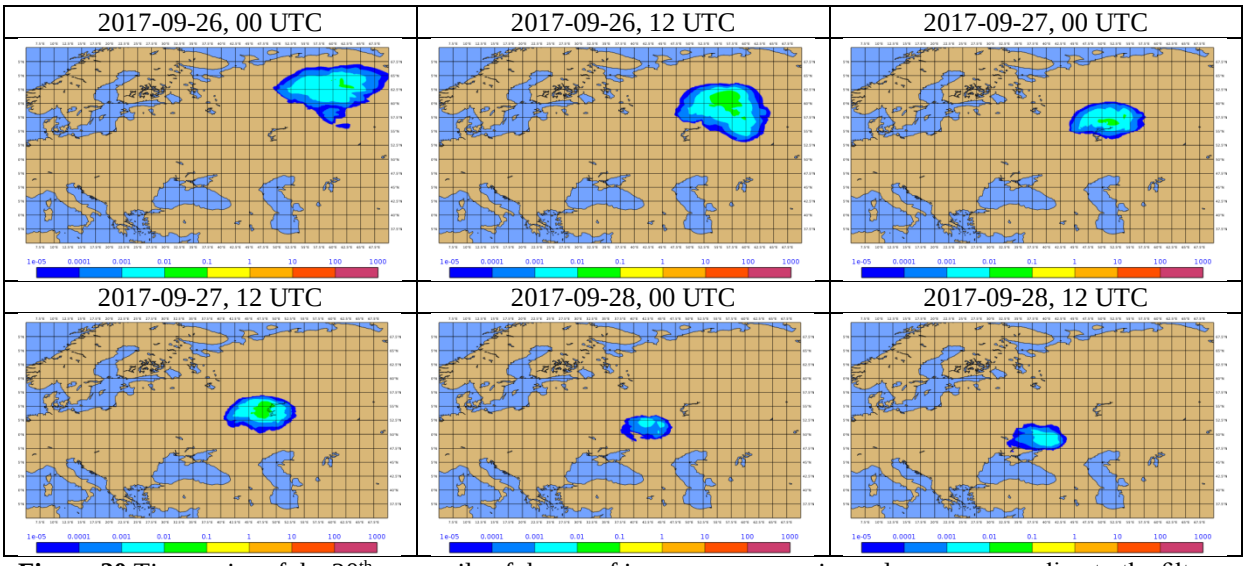

Figure 20 Time series of the 20th percentile of the set of inverse concentration values corresponding to the filter station measurements.

The time series of these 20th percentile maps has been combined in one plot in the left-hand side of Figure 21 which thereby depicts the estimate of the potential location of the release of Ru-106. The release point is thus expected to be located inside a narrow geographic zone ranging from around Perm and Yekaterinburg in the north-east to Odessa in the south-west. In the right-hand side is shown the corresponding figure using the 30th percentile maps. The larger the percentage used for the percentile, the larger the disagreement is accepted between the individual inverse concentration calculations corresponding to measured values.

For operational use, the best (lowest) percentage used for the quantile calculation is not known a priori. The value depends both on the distribution of the measured concentration values and on how well-conditioned the problem is, i.e. how well the observations match the plume geographically and temporally. Thus, the recommendation is to calculate a range of percentiles which is anyway cheap from a computational point of view. In near real time in an operational environment, the problem is likely to be ill-conditioned at the early phase where only few measurements are available.

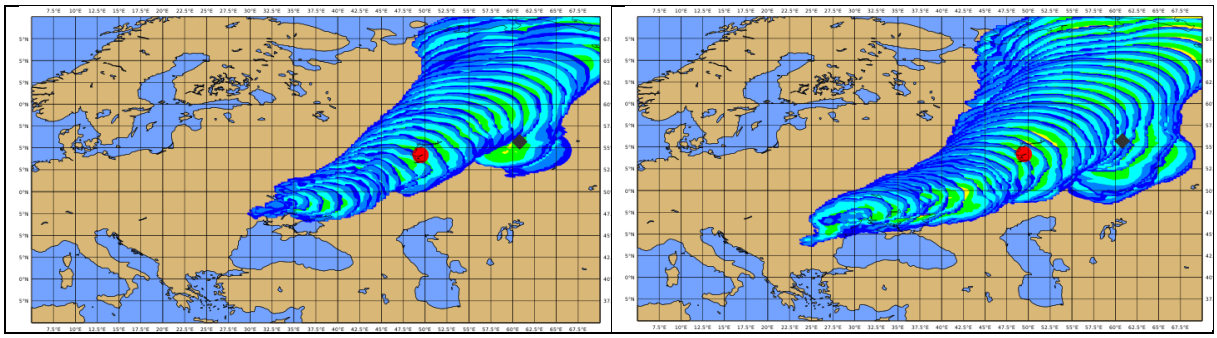

Figure 21 Estimates of the potential location of the release of Ru-106. The release point is located within a geographic zone ranging from around Perm and Yekaterinburg in the north-east to Odessa in the south-west. The left-hand figure consists of the overlapping time series of three-hourly 20th percentile inverse concentration maps from 2017-09-25 00 UTC to 2017-09-29 15 UTC, the right-hand figure consists of 30th percentile maps from 2017-09-25 00 UTC to 2017-09-30 18 UTC. With a red dot and a black diamond, the NIIAR and the Mayak nuclear facilities are indicated, respectively.

The geographic zones depicted in Figure 21 agree well with the corresponding zone estimated by a different method by Institut de Radioprotection et de Sûreté Nucléaire (IRSN, 2017). However, the method presented in the current paper is probably less computer resource demanding than the IRSN method.

It has been suggested that the release site could be the NIIAR nuclear facility, JSC "SSC RIAR", Russian Federation, 433510, Ulyanovsk region, Dimitrovgrad, Zapadnoye Shosse 9, cf. http://www.niiar.ru. If this is so, then according to the time series of the inverse model results, the release should have taken place within the time period 0–16 UTC on 2017-09-27. Likewise, it has been suggested that the release could be the Mayak Production Association, Russian Federation, Ozersk, Tjeljabinsk oblast, Lenin str. 31, cf. http://www.po-mayak.ru/. If so, according to the inverse model results, the release should have taken place in the time period 5–13 UTC on 2017-09-26.

Results of MATCH

Both Markov Chain Monte Carlo and percentiles for individual plumes were applied to the Ru-106 case in 2017, using the MATCH model.

Markov Chain Monte Carlo

The MCMC approach was applied having starting points in three locations: Dimitrovgrad, Mayak and an additional position in between. The full dataset (387 measurements) of various sampling integration times where used. The approach converges in all cases but end rather close to the starting point. The additional point in between Dimitrovgrad and Mayak converge to more or less the same location as when starting in Mayak. Figure 22 shows the results for these three evaluations. Making a step to Figure 24 and percentiles of time-integrated total columns there is a signal that both Dimitrovgrad and Mayak may be possible release sites, being on a path of max percentile values. The MCMC approach very much search towards a nearby point on this path of max values that falls within a similar emission time-profile as for the starting point in the MCMC procedure.

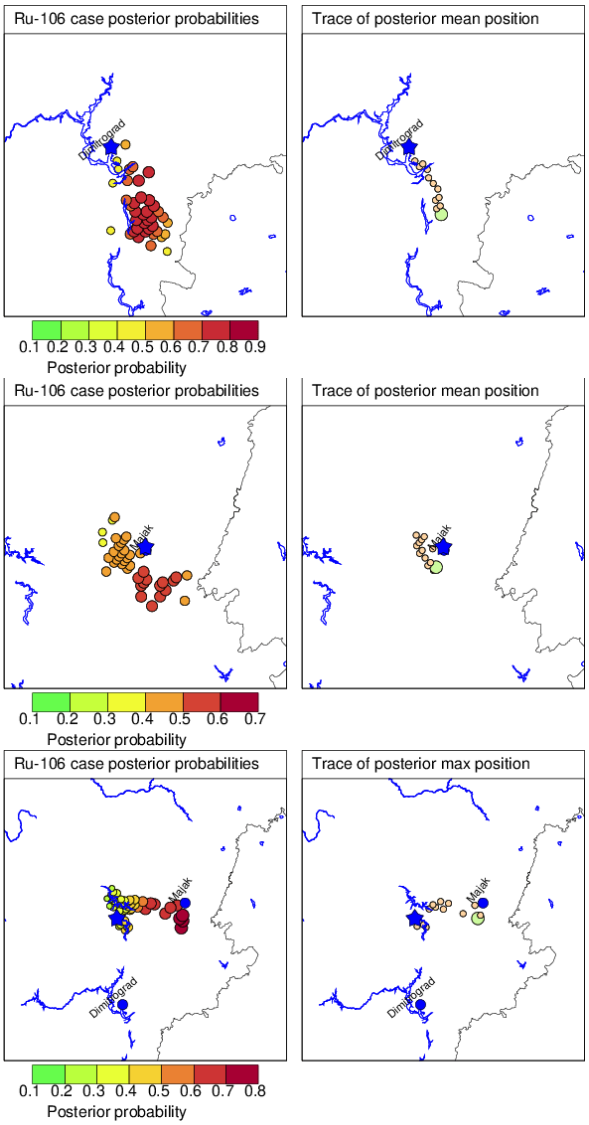

Figure 22 Markov Chain Monte Carlo simulations for Dimitrovgrad (top) and Mayak (middle), and a location in between these sites (bottom). Posterior probabilities for visited locations are shown to the right and the mean path thru the iterations are shown to the left (for the bottom case max position trace became more informative). The starting point for MCMC is marked with a blue star, and the end point with a green bullet.

Percentiles for individual plumes

The percentile approach was as for the ETEX-I case evaluated on a reduced set of measurements. From in total 387 measurements a set of 131 did provide measurements with up to 36 hours sampling times. From this latter sub-set 30 measurements were depicted. The first 10 with highest measured values were taken and the remaining 20 were randomly selected by weighted bootstrapping (conditional on measured values). Figure 23 shows all the sites for the 131 measurements (left) and the used sites with the selected 50 measurement (right).

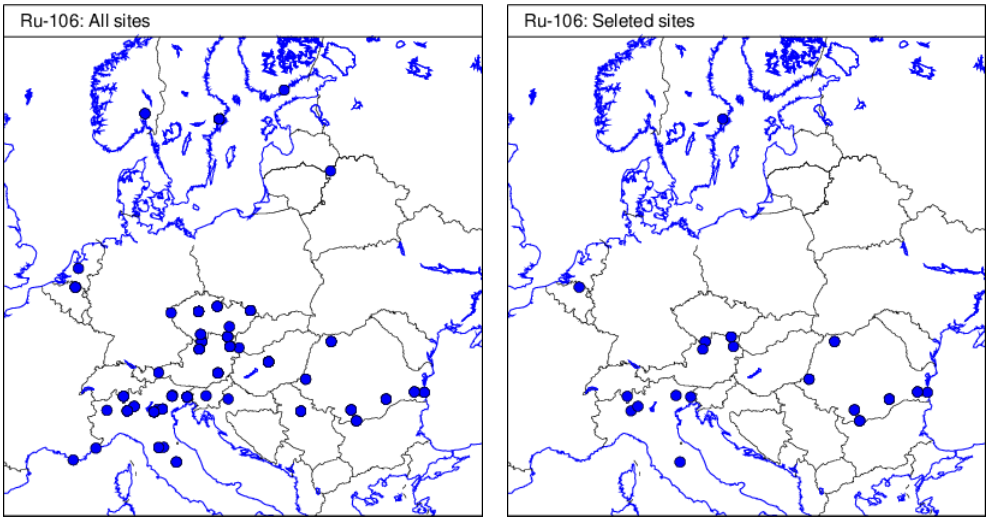

Figure 23 All sites provided from IAEA providing measurement with up to 36 hours sampling times (left) and the selected ones (right).

Individual plumes were made for each measurement with a unit response assumed valid over a depth of 50 m and distributed over the time-interval for the measurement (ranging from 7 to 36 hours). In post processing, each inverse plume was scaled by measured value associated with the plume.

Figure 24 shows the 70th percentile of total columns as well as 70th percentiles of time-integrated total columns for the 25, 27 and 28 September, 2017. The total column is selected to include a vertical extension of the source. The percentiles of time-integrated columns should be interpreted as showing possible source location at any time back to the date plotted. This covers a larger area for the Ru-106 case but showing max values in a band from Italy, Ukraine and southern Russia. The plotted dates are selected to illustrate approximate dates for any releases at Dimitrovgrad and Mayak.

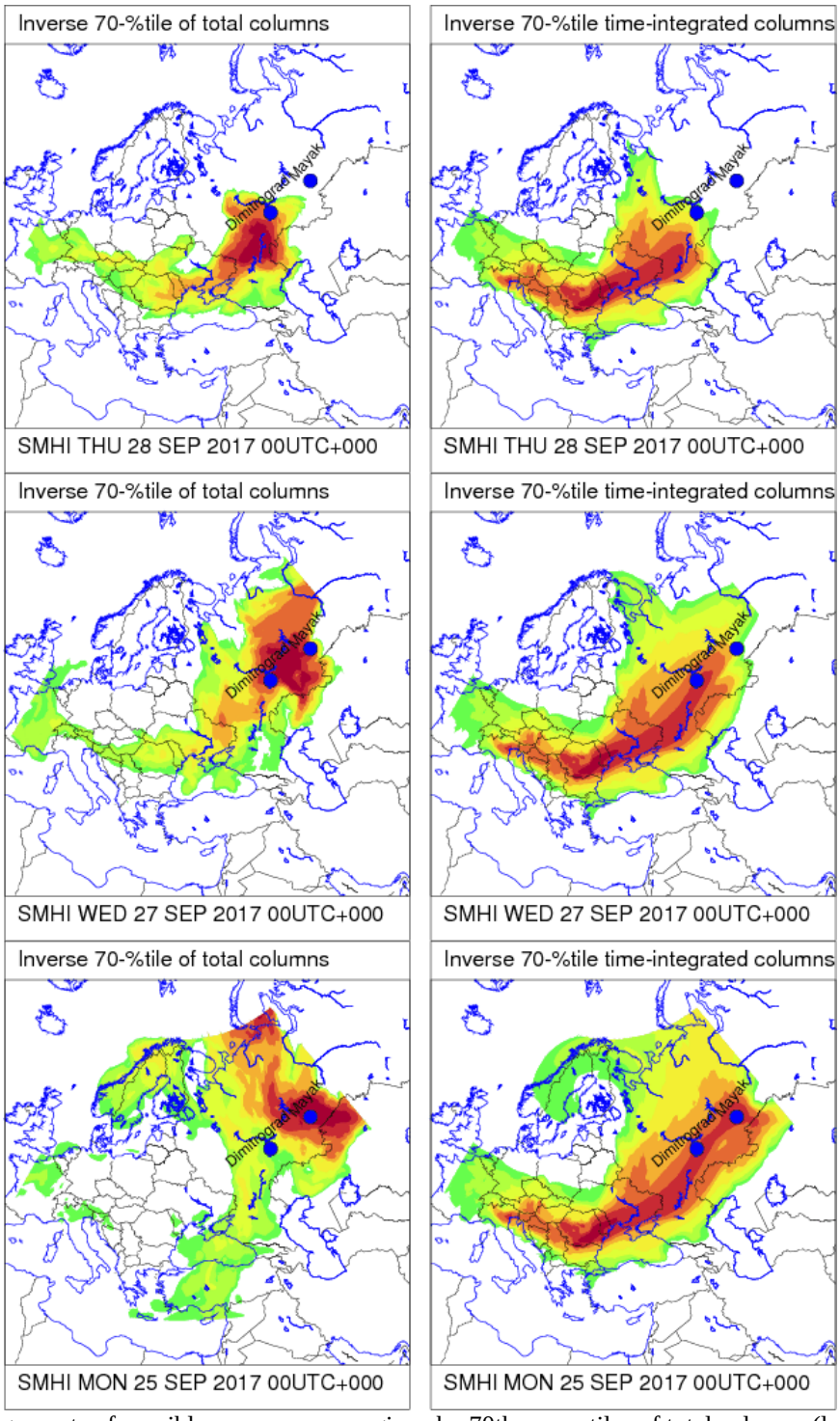

Figure 24 Assignments of possible source areas as given by 70th percentiles of total columns (left) and 70th percentile of time-integrated total columns (right). The percentiles are normalised to simplify plotting. Dates plotted are 28 Sep 00 UTC, 2017 (top), 27 Sep 00 UCT (middle) and 25 Sep 00UTC (bottom). The locations for Dimitrovgrad and Mayak are plotted.

Results of SNAP

For the Ruthenium case, all 383 measurements, shown in Figure 25 were used, combining both the measurements below LOD and detections. The adjoint model was run back until 2017-09-22, 03 UTC. Figure 26 shows the maximal probabilities along with the development in time of the probability densities. The areas of high probability cover a larger area than for the ETEX case, making an estimate for source location coarser.

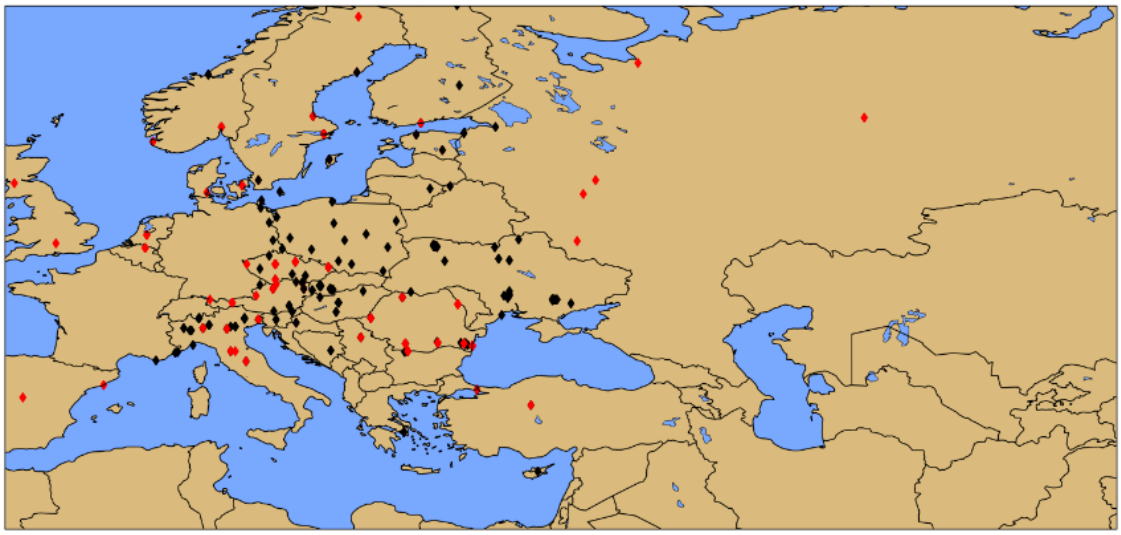

Figure 25 Location of stations in the Ruthenium case. Red diamonds show stations with measurements below LOD, black diamonds show measurements above LOD.

Examining different release durations gives Figure 27, showing the maximum probability densities for longer release durations than shown in Figure 26. The smaller area of the highest probabilities (dark red) for the two hour release duration, and much smaller areas for ten hours suggest a source lasting for only a short duration.

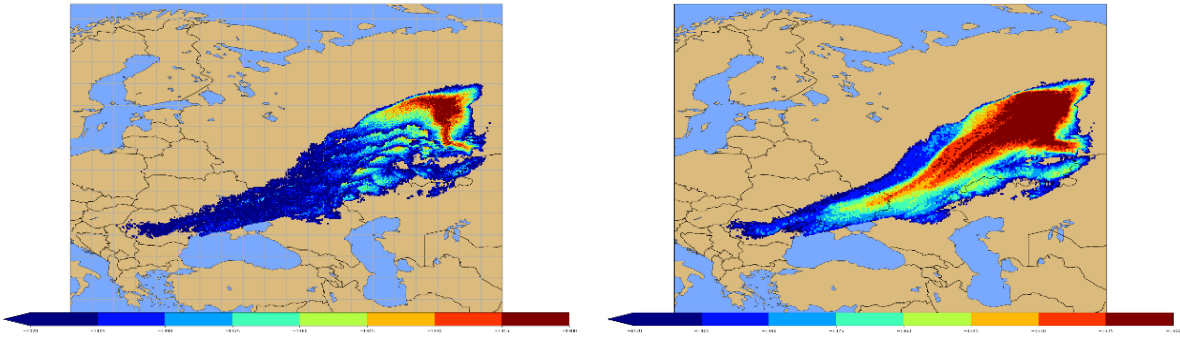

Figure 26 Probability densities assuming a one hour duration of the release for the period 2017-09-26, 00 UTC – 2017-09-28, 15 UTC. On the left slices of probability densities for every sixth hour are shown. On the right the maximum probability densities are presented.

The larger spread in probability densities could be a result of different thresholds and LOD for the various stations, compared to the more homogenous ETEX case, suggesting the probabilities used should be dynamic per station, and scale with the dilution volume. The deterministic meteorological model used in the simulations does not capture any meteorological uncertainty, which might affect the long-range transport severely.

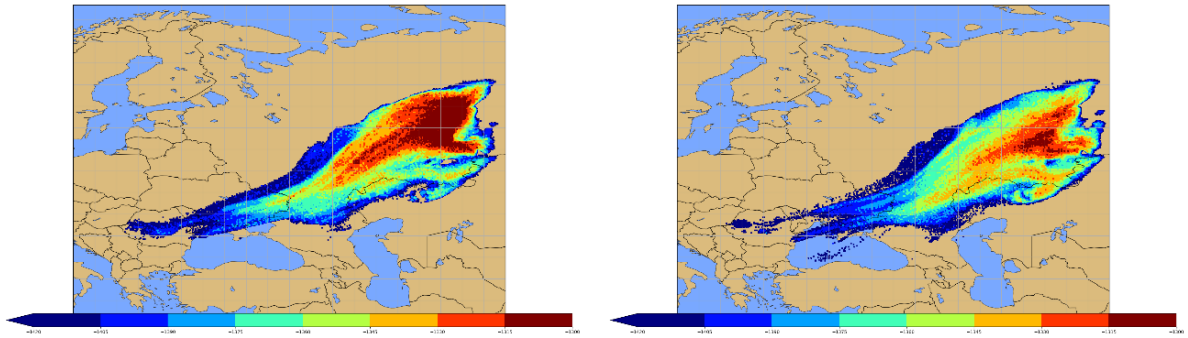

Figure 27 Maximum probability densities between 2017-09-26, 00 UTC - 2017-09-28, 15 UTC, assuming a two hour release duration on the left, and a ten hour release duration on the right.

ARGOS and Source Localization

The Long Range dispersion model interface in ARGOS is now capable of providing an ensemble of source terms – a list of possible release descriptions for the same accident type – and to handle multiple results from a single Long Range (LR) request, including a set of statistical results from a so-called 'Ensemble' run.

This new feature is implemented in collaboration with the Danish Meteorological Institute (DMI) on whose HPC facility a single model run request from ARGOS in parallel produces a number of deterministic results (each in its own file) and a number of statistical results (all in the same file) – all based on the same input request but with differing source terms – from the ensemble of source terms – and with different versions of NWP model data. Statistical results will be available for the ensemble of NWP model data for each source term and for the combination of all source terms and all NWP model data.

Concentration Measurements in ARGOS

The ARGOS-DSS features several different options for visualising different kinds of radiological measurements. An example is shown below where a plot of European Monitoring Stations is presented in ARGOS. Station data are imported using the EURDEP-protocol, see Figure 28.

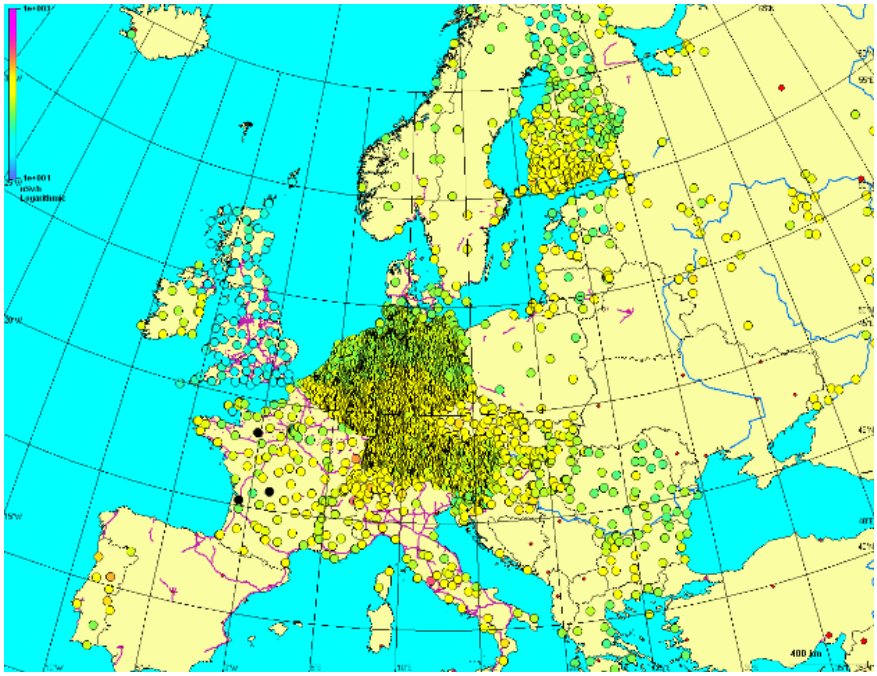

Figure 28 European Monitoring Stations presented in ARGOS.

The typical output from these types of Permanent Monitoring Stations is a dose rate; normal unit µSv/h.

Likewise, ARGOS is capable of importing and presenting data from Air Sample Stations – again importing data using the EURDEP-protocol. Typical output from these Air Sample Stations is an air concentration; normal unit Bq/m^3 (per nuclide).

Request for Source Localization Calculation from ARGOS

The existing Request dialog in ARGOS today is focused on doing forward Atmospheric Dispersion modelling; giving the user options for selecting a release point (a reactor) and a release description (source term – or ensemble of source terms) and a release time, see Figure 29.

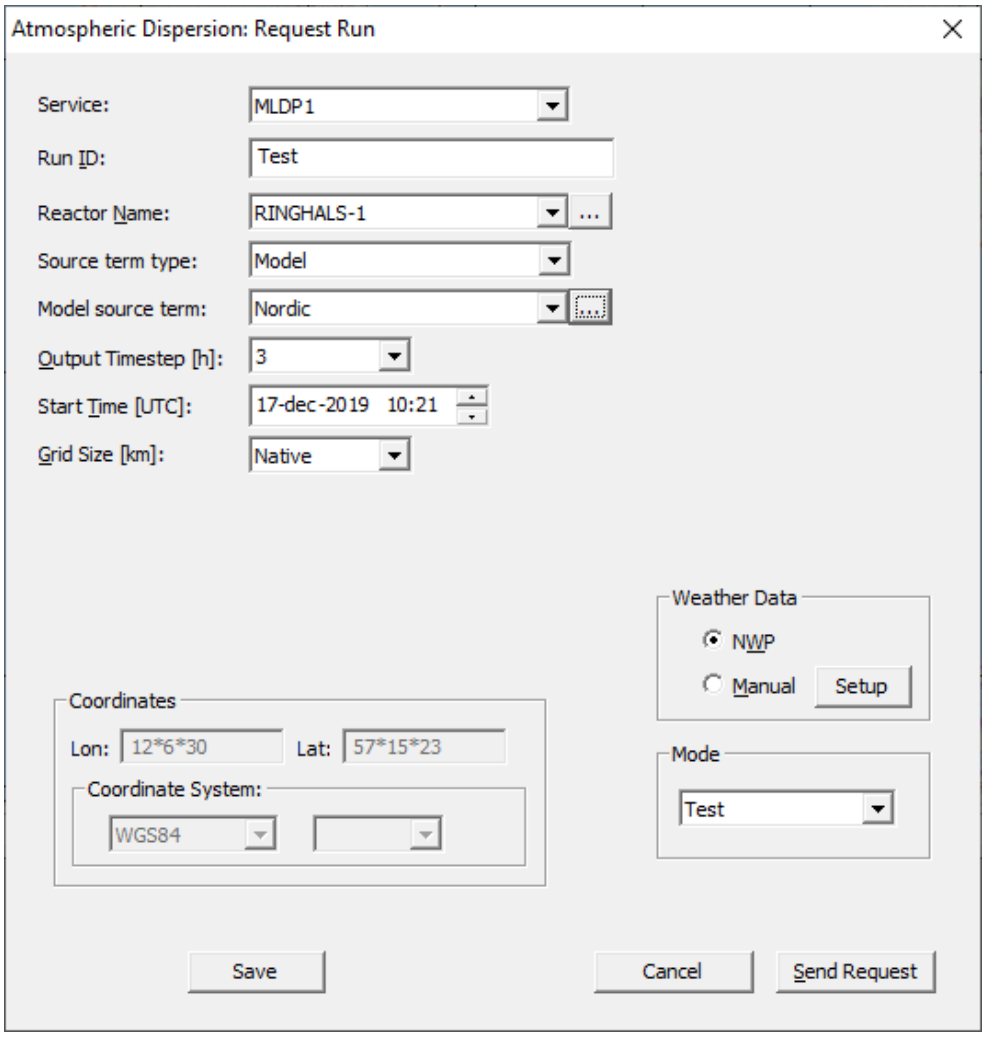

Figure 29 Forward atmospheric dispersion modelling request dialog in ARGOS.

For Source Localization Calculations (SLC) the needs are quite different from (normal) forward ADM. The user needs to provide a (number of) detection(s) of time-average air concentrations to be part of the request send to the model. As ARGOS already today have a module for presenting different measurements in the system (see section above) it would be natural to base the GUI for requesting SLC on the existing GUI for selecting measurement data to be visualized in the system. Due to the number of different types of measurement data, the GUI for selection is rather complicated, see Figure 29.

The needs for SLC can be narrowed down to these three parameters:

- The area of interest – the area where the system should select measurement data
- The time frame of interest – the time period where the system should select measurement data
- The type of measurements

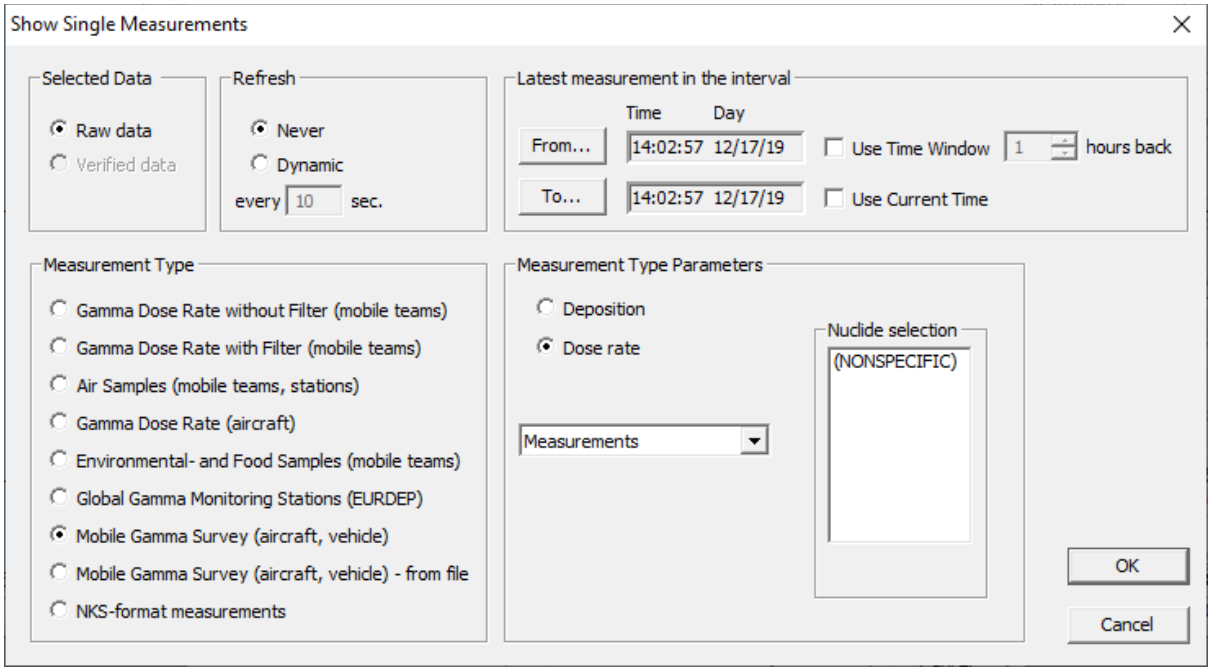

Figure 30 GUI for selecting measurement data to be visualized in the system.

Area of interest

The easiest way of defining the Area Of Interest (AOI) is to simply use the current map selection in the system – the part of the map that the user is viewing when the request is made. As an alternative, one could consider providing the user with the option of defining the AOI explicit; giving the specific coordinates of the lower left and upper right corners of the AOI. Whereas, using traditional selections of AOI such as a radius around a release point has been deemed obsolete in this case; as there is no (known) release point.

Time period of interest

The simple setting of a "From time" and a "To time" will be maintained as the mean of selecting the time frame for sampling measurements that the system should select data for.

Do note that such a selection is necessary as some organizations are using their ARGOS installation as the primary source of storing (historical) measurement data. Thus the system can have measurement data for an arbitrary period back in time. However, when requesting a SLC, one will only have to provide data for the period in which elevated concentrations are recorded by at least part of the stations.

As Air Sampler Stations typically have substantial sampling periods, one will have to ensure that these periods are fully covered by the overall time period of interest.

Types of measurements

As can be seen from the GUI for visualising measurements in ARGOS above, ARGOS can handle quite many types of measurements. In order to simplify the GUI, we will restrict the selection for SLC to be limited to:

- Permanent Monitor Stations – dose rates
- Air Sampler Stations – air concentrations

Or a combination of the two.

It has to be considered how to distinguish between “lack of data” from a station and “below detection limit measurements”. Of course, in the radiological domain there will always be some background radiation.

Permanent gamma-monitors and filter stations

In Europe, many radiological filter station measurements are taken once a week. However, in special cases it is possible to change to daily measurements. From a meteorological perspective, a week can be a long time covering a number of different meteorological phenomena taking place over the station site within the period. Additionally, a week could be longer than the accidental release. Thus, if the intended use of the measurements among other things is to assist in locating the release point, daily measurements are of much greater value. The filters are changed manually, and in most cases sent by regular mail for analysis. This implies a delay in retrieving the measurement data, and it means that short-lived radionuclei have decayed when the filter is measured.

The detection limit depends first of all on the amount of air drawn through the filter. Thus, the pump efficiency and the measurement period are key parameters for the detection limits, and therefore detection limits vary across Europe. In addition, the presence of many radionuclei on a filter makes it difficult to measure concentrations accurately.

There are currently no international agreements on routine distribution of filter station concentration measurements. For the October 2017 case of Ru-106 measurements in Europe, the IAEA collected the available filter station data. There are, however, problems with this data set e.g. regarding the time stamps which are not well defined in all cases.

The European Radiological Data Exchange Platform (EURDEP) is a network for the exchange of radiological monitoring data between most European countries. Currently, EURDEP is used for the European automatic gamma monitoring network which does not provide activity concentrations, only gamma dose rates. However, EURDEP might be used also for filter station measurements which could be very helpful in future events.

In comparison with filter-stations, the gamma monitoring network in Europe is much denser and reports automatically at high frequency, e.g. hourly, all of which make such data attractive for an operational nuclear DSS. However, in order to use the gamma-monitoring data for inverse modelling it is required that measurements of nuclide-specific average activity concentrations are provided. Further, the measurement sensitivity is several orders of magnitude worse than for filter stations. Thus, gamma monitoring results are most likely only useful for source localization at the early phase of a nuclear accident.

The Comprehensive Nuclear-Test-Ban Treaty Organization (CTBTO) includes a monitoring network of 80 radiological stations measuring radioactive particles, around half of them also noble gasses. Near real time access to these data will be helpful for locating an unknown release of radionuclei.

Presenting results from Source Localization Calculation in ARGOS

As part of the AVESOME-project the concept of presenting model results to the user in the form of time dependent probability plots was introduced together with the ability of dealing with so-called Percentile plots. This ability will be re-used to present the results from the SLC-modelling. In order to assist the user in pinpointing potential release sites, these plots can be superimposed with the ARGOS-database of nuclear facilities, see Figure 31.

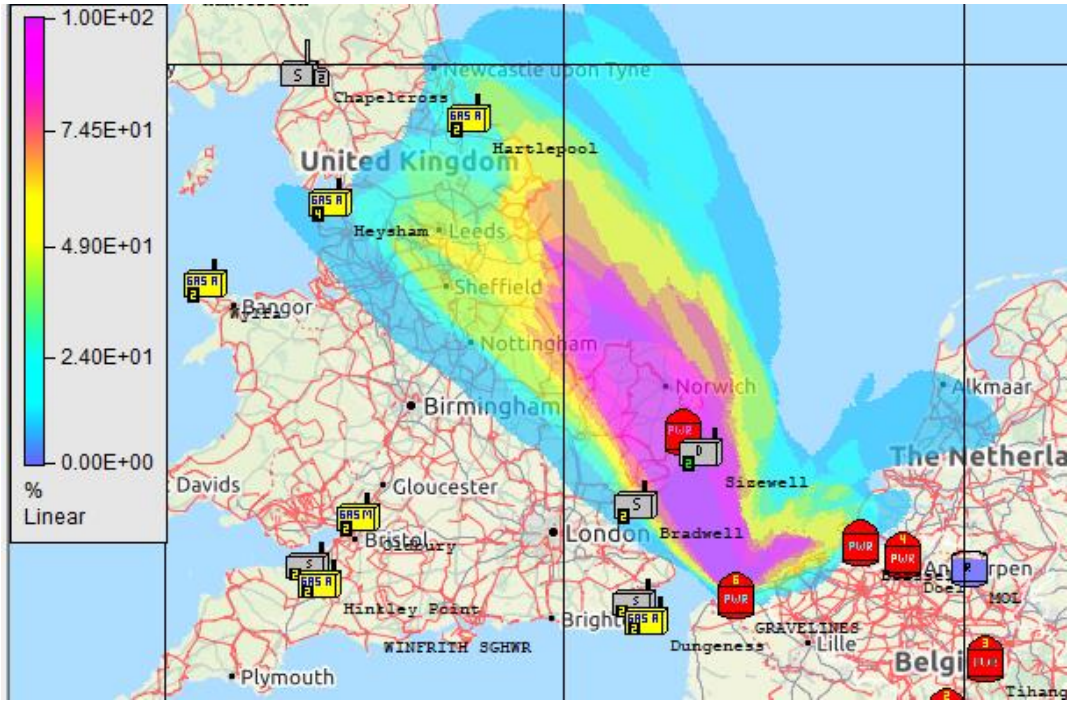

Figure 31 ARGOS presentation of probabilistic forward atmospheric dispersion model results superimposed by nuclear facilities.

Conclusions and Outlook

Various methods for localization of an unknown source of radionuclides, which have been accidentally released to the atmosphere, are developed employing measurements of activity concentrations. The methods have been applied to two cases, viz. the European Tracer Experiment (ETEX) and the October 2017 case of Ru-106 in Europe. The atmospheric dispersion models DERMA, MATCH and SNAP have been used in adjoint mode making use of deterministic numerical weather prediction model data derived from the global model of the European Centre for Medium-Range Weather Forecasts (ECMWF).

From the given set of measured concentrations, inverse instantaneous activity concentration fields are calculated by the dispersion models. A level of agreement method, described in terms of percentiles, is applied to the overlap of these inverse concentration fields, whereby localization of the unknown source is provided for expert judgement in terms of geographic areas and release time periods. Another method utilises a simplified Bayesian approach on the set of inverse concentration calculations benefitting from both detection and non-detection measurements. Depending on the measured concentrations, the overlap areas and periods can be more or less extensive. Finally, the Markov Chain Monte Carlo approach could be a last refinement, but in this case a qualified first guess of the source location has to be at hand.

For the two selected cases, the available filter-station measurements are used. This mimics the situation at a late phase of an accidental release of radionuclides. At the early stage of an event, however, measurements will probably be available only from gamma monitoring networks. In this case, one should expect to have only gamma dose rates available given as the total of the various radionuclides released. Unfortunately, dose rates are not directly applicable by all methods, since nuclide-specific concentration measurements are necessary to initialize the inverse models.

Treating the measured dose rates as concentrations can, however, be sufficient for source localization purposes. Such treatment of dose rates can be justified when the dose rate is dominated by a single radionuclide or by a family of radionuclides where the half-lives are comparable and similar for the dose conversion factors. In this case, the dose rates are approximately proportional to activity concentrations. Without knowledge on nuclide composition, the dose rates can e.g. be treated as concentrations of a non-depositing inert species without decay.

The gamma stations in Europe are numerous and positioned densely, and they report frequently, e.g. hourly, and automatically, all of which makes them attractive for source localization purposes. A disadvantage, however, is the detection limit, which is not as fine as for filter stations. Thus, especially in the early phase of an accidental release, gamma stations not too far from the release site may be useful. In a later phase, filter station data including stations far from the release site should replace the use of gamma station data.

In the anticipated continuation of the SLIM project, the effects of the inherent meteorological uncertainties will be quantified by incorporating the MUD methodology (Sørensen *et al.*, 2014) in the inverse modelling approach. In addition, methods for estimating the emission profile for the various radionuclides detected should be developed for the locations that the various SLIM approaches point out to be of interest. These methods must be suited for operational use in nuclear DSSs, and they should include estimates of the inherent uncertainties.

References

Andersson, C., Bergström, R., Bennet, C., Robertson, L., Thomas, M., Korhonen, H., Lehtinen, K.E.J., and Kokkola, H. 2015. MATCH-SALSA – Multi-scale Atmospheric Transport and CHemistry model coupled to the SALSA aerosol microphysics model – Part 1: Model description and evaluation. *Geosci. Model Dev.* **8**, 171–189. doi:10.5194/gmd-8-171-2015

Baklanov, A. and J. H. Sørensen. Parameterisation of radionuclide deposition in atmospheric dispersion models. *Phys. Chem. Earth* **26** (2001) 787–799

Baklanov, A., A. Mahura and J. H. Sørensen. Methodology for Prediction and Estimation of Consequences of Possible Atmospheric Releases of Hazardous Matter: 'Kursk' Submarine Study. Atmos. *Phys. Chem.* Vol. **3** (2003) 747–762

Bartnicki, J., H. Haakenstad, and Ø. Hov. Operational SNAP model for remote applications from NRPA. *Norwegian Meteorological Institute Report* (2011) 12–2011

Bartnicki, J., I. Amundsen, J. Brown, A. Hosseini, Ø. Hov, H. Haakenstad, H. Klein. Atmospheric transport of radioactive debris to Norway in case of a hypothetical accident related to the recovery of the Russian submarine K-27. *Journal of environmental radioactivity* **151** (2016) 404–416

Bengtsson, L., U. Andrae, T. Aspelien, Y. Batrak, J. Calvo, W, de Rooy, E. Gleeson, B. H. Sass, M. Homleid, M. Hortal, K.-I. Ivarsson, G. Lenderink, S. Niemelä, K. P. Nielsen, J. Onvlee, L. Rontu, P. Samuelsson, D. S. Muñoz, A. Subias, S. Tijm, V. Toll, X. Yang, and M. Ø. Køltzow. The HARMONIE–AROME Model Configuration in the ALADIN–HIRLAM NWP System. *Monthly Weather Review* (2017) **145** No. 5 https://doi.org/10.1175/MWR-D-16-0417.1

ETEX web-site (2019), https://rem.jrc.ec.europa.eu/etex/

Gloster, J., A. Jones, A. Redington, L. Burgin, J. H. Sørensen, R. Turner. International approach to atmospheric disease dispersion modelling. *Veterinary Record* 03 (2010a) **166** (12):369. DOI:10.1136/vr.166.12.369a

Gloster, J., A. Jones, A. Redington, L. Burgin, J. H. Sørensen, R. Turner, P. Hullinger, M. Dillon, P. Astrup, G. Garner, R. D'Amours, R. Sellers and D. Paton. Airborne spread of foot-and-mouth disease – model intercomparison. *Veterinary Journal* **183** (2010b) 278–286

Graziani, G., Klug, W., and Nodop, K. Real-time Long-range Dispersion Model Evaluation of the ETEX First Release. **EUR 17754 EN** (1998) 92-828-3657-6 European Commission

Hastings, W. (1970). Monte Carlo sampling methods using Markov chains and their applications. *Biometrika* 57 (1), 97–109

Hoe, S., J. H. Sørensen and S. Thykier-Nielsen. The Nuclear Decision Support System ARGOS NT and Early Warning Systems in Some Countries around the Baltic Sea. In: Proceedings of the 7th Topical Meeting on Emergency Preparedness and Response, September 14–17, 1999, Santa Fe, New Mexico, USA

Hoe, S., H. Müller, F. Gering, S. Thykier-Nielsen and J. H. Sørensen. ARGOS 2001 a Decision Support System for Nuclear Emergencies. In: Proceedings of the Radiation Protection and Shielding Division Topical Meeting, April 14–17, 2002, Santa Fe, New Mexico, USA

IAEA. Convention on Early Notification of a Nuclear Accident. (1986) https://www.iaea.org/publications/documents/treaties/convention-early-notification-nuclear-accident

IAEA. Updated Technical Attachment Status of Measurements of Ru-106 in Europe, 2017-10-20, 12:00 UTC, prepared by the Incident and Emergency Centre of the IAEA. Available through national radiation protection authorities.

IRSN. Detection of Ruthenium 106 in France and in Europe: Results of IRSN's investigations. November 9, 2017 http://www.irsn.fr/EN/newsroom/News/Documents/IRSN_Information-Report_Ruthenium-106-in-europe_20171109.pdf

Kahnert, M., Variational data analysis of aerosol species in a regional CTM: Background error covariance constraint and aerosol optical observations operators, *Tellus*, 60B, 753-770, (2008)

Kahnert, M. (2018). Information constraints in variational data assimilation. *Q. J. R. Meteorol. Soc.* 144, 2230-2244

Keats, A., Yee, E., and Lien, F.-S. (2006). Bayesian inference for source determination with application to complex urban environment. *Atmospheric Environment,* 41, 465–479

Keats, A., Yee, E., Lien, F.-S., and D'Amours, R. (2008). Bayesian inversion of concentration data: Source reconstruction in the adjoint representation of atmospheric diffusion. *Journal of Wind Engineering,* 96, 1895–1816.

Klein, H., and Bartnicki**,** J. (2018). The Severe Nuclear Accident Programme, Concert Air2 Bulletin, Issue 24, 2018, page 4

Lauritzen, B., A. Baklanov, A. Mahura, T. Mikkelsen and J. H. Sørensen. K-model description of probabilistic long-range atmospheric transport in the Northern Hemisphere. *Atmos. Environ.* **40** (2006) 4352–4369

Lauritzen, B., A. Baklanov, A. Mahura, T. Mikkelsen and J. H. Sørensen. Probabilistic risk assessment for long-range atmospheric transport of radionuclides. *J. Envir. Radioactivity* **96** (2007) 110–115

Mahura, A., A. Baklanov and J. H. Sørensen. Methodology for evaluation of possible consequences of accidental atmospheric releases of hazardous matter. *Radiat. Prot. Dos.* **103** (2003) 131–139

Mahura, A. G., A. A. Baklanov, J. H. Sørensen, F. L. Parker, V. Novikov, K. Brown, K. L. Compton 2004: Assessment of Atmospheric Transport and Deposition Patterns Related to Russian Pacific Fleet Operations. *Environmental Monitoring and Assessment* **101** (2005) 261–287

Pudykiewicz, J. A. Application of adjoint tracer transport equations for evaluating source parameters. *Atmos. Environ.* **32** (1998) 3039–3050

Rao, S. Source estimation methods for atmospheric dispersion. *Atmos. Environ.* **41** (2007) 6964–6973

Mikkelsen, T., S. Alexandersen, H. Champion, P. Astrup, A. I. Donaldson, F. N. Dunkerley, J. Gloster, J. H. Sørensen and S. Thykier-Nielsen. Investigation of Airborne Foot-and-Mouth Disease Virus Transmission during Low-Wind Conditions in the Early Phase of the UK 2001 Epidemic. *Atmos. Chem. Phys. Disc.* **3** (2003) 677–703

PDC-ARGOS. http://www.pdc-argos.com

Robertson, L. and Langner, J. 1998. Source function estimate by means of variational data assimilation applied to the ETEX-1 tracer experiment. *Atmos. Environ.* **32**, 4219-4225

Robertson, L., Langner, J. and Engardt, M., An Eulerian limited-area atmospheric transport model, *J. Appl. Met.* 38, 190-210, 1999.

Robertson, L. 2004. *Extended back-trajectories by means of adjoint equations.* Swedish Meteorological and Hydrological Institute, **RMK No. 105**, 37 pp.

Saltbones, J., A. Foss, and J. Bartnicki. Norwegian Meteorological Institute's real-time dispersion model SNAP (Severe Nuclear Accident Program): Runs for ETEX and ATMES II experiments with different meteorological input. *Atmospheric Environment* **32** no. 24 (1998) 4277-4283

Seibert, P. Methods for source determination in the context of the CTBT radionuclide monitoring system. In: Proceedings Informal Workshop on Meteorological Modelling in Support of CTBT Verification, Vienna (2000)

Seibert, P. Inverse modelling with a Lagrangian particle dispersion model: application to point releases over limited time intervals. In: Gryning, S.E., Schiermeier, F.A. (Eds.), Air Pollution Modeling and its Application XIV (2001) Plenum Press, New York, pp. 381–389

Seibert, P. Inverse modelling of atmospheric trace substances on the regional scale with Lagrangian models. In: Proceedings of the EUROTRAC-2 Symposium, 11–15 March 2002, Garmisch-Partenkirchen, Germany (2002)

Senocak, I., N. W. Hengartner, M. B. Short, and W. B. Daniel. Stochastic event reconstruction of atmospheric contaminant dispersion using Bayesian inference. *Atmospheric Environment* **42** no. 33 (2008) 7718-7727

Smith, A., and Gelfand, A. (1992). Bayesian statistics without tears: A sampling-resampling

perspective. *The American Statistician*, 42 (2), 84–88.

Sørensen, J. H. Method for source localization proposed and applied to the October 2017 case of atmospheric dispersion of Ru-106. *Journ. Envir. Radioactivity* **189C** (2018) 221–226 https://doi.org/10.1016/j.jenvrad.2018.03.010 https://www.sciencedirect.com/science/article/pii/S0265931X18300146

Sørensen, J. H. Sensitivity of the DERMA Long-Range Dispersion Model to Meteorological Input and Diffusion Parameters. *Atmos. Environ.* **32** (1998) 4195–4206

Sørensen, J. H., D. K. J. Mackay, C. Ø. Jensen and A. I. Donaldson. An integrated model to predict the atmospheric spread of foot-and-mouth disease virus. *Epidemiol. Infect.* (2000) 124, 577–590

Sørensen, J. H., C. Ø. Jensen, T. Mikkelsen, D. Mackay and A. I. Donaldson. Modelling the atmospheric spread of foot-and-mouth disease virus for emergency preparedness. *Phys. Chem. Earth* **26** (2001) 93–97

Sørensen, J. H., A. Baklanov and S. Hoe. The Danish Emergency Response Model of the Atmosphere. *J. Envir. Radioactivity* **96** (2007) 122–129

Sørensen, J. H., B. Amstrup, H. Feddersen, U. S. Korsholm, J. Bartnicki, H. Klein, P. Wind, B. Lauritzen, S. C. Hoe, C. Israelson, and J. Lindgren. Meteorological Uncertainty of atmospheric Dispersion model results (MUD). **NKS-307** ISBN 978-87-7893-385-0, http://www.nks.org/en/nks_reports/view_document.htm?id=111010212220490 (2014)

Sørensen, J.H., B. Amstrup, H. Feddersen, J. Bartnicki, H. Klein, M. Simonsen, B. Lauritzen, S. C. Hoe, C, Israelson and J. Lindgren. Fukushima Accident: UNcertainty of Atmospheric dispersion modelling (FAUNA). **NKS-360** ISBN 978-87-7893-444-4 (2016), http://www.nks.org/scripts/getdocument.php?file=111010213440189

Sørensen, J. H., B. Amstrup, T. Bøvith, H. Feddersen, R. Gill, M. Sørensen, F. Vejen, P. Astrup, N. Davis, B. Lauritzen, S. C. Hoe, J. E. Dyve, P. Lindahl. MEteorological uncertainty of ShOrt-range dispersion (MESO). **NKS-380** ISBN 978-87-7893-466-6 (2017), http://www.nks.org/en/nks_reports/view_document.htm?id=111010214043891

Sørensen, J. H., Schönfeldt, F., Sigg, R., Pehrsson, J., Lauritzen, B., Bartnicki, J., Klein, H., Hoe, S. C., and Lindgren, J. Added Value of uncertainty Estimates of SOurce term and Meteorology (AVESOME) – final report. NKS-420, ISBN 978-87-7893-509-0 (2019) http://www.nks.org/en/nks_reports/view_document.htm?id=111010214696230

Wotawa, G., L.-E. De Geer, P. Denier, M. Kalinowski, H. Toivonen, R. D'Amours, F. Desiato. Atmospheric transport modelling in support of CTBT verification—Overview and basic concepts. *Atmospheric Environment* **37**, no. 18 (2003) 2529-2537

Yee, E. (2008). Automated computational inference engine for Bayesian source reconstruction: Application to some detections/non-detections made in the CTBT International Monitoring System. *Journal of Wind Engineering* **96** 1895–1816.

Yee, E. (2012). Probability theory as logic: Data assimilation for multiple source reconstructions. *Pure Applied Geophysics* **169** 499–517.

Yee, E. Automated computational inference engine for Bayesian source reconstruction: Application to some detections/non-detections made in the CTBT International Monitoring System. *Applied Mathematical Sciences* **11** no. 32 (2017) 1581-1618.

Acknowledgements

NKS conveys its gratitude to all organizations and persons who by means of financial support or contributions in kind have made the work presented in this report possible.

Disclaimer

The views expressed in this document remain the responsibility of the author(s) and do not necessarily reflect those of NKS. In particular, neither NKS nor any other organisation or body supporting NKS activities can be held responsible for the material presented in this report.

Bibliographic Data Sheet **NKS-430**

Title	Source Localization by Inverse Methods (SLIM)
Author(s)	Jens Havskov Sørensen[1] (co-ordinator) Heiko Klein[2] Magnus Ulimoen[2] Lennart Robertson[3] Jan Pehrsson[4] Bent Lauritzen[5] Dan Bohr[6] Agnieszka Hac-Heimburg[6] Carsten Israelson[6] Anna Maria Blixt Buhr[7] Jonas Lindgren[7] Tero Karhunen[8] Tuomas Peltonen[8]
Affiliation(s)	[1]Research and Development Department, Danish Meteorological Institute (DMI) [2]Norwegian Meteorological Institute (MET Norway) [3]Swedish Meteorological and Hydrological Institute (SMHI) [4]PDC-ARGOS [5]Center for Nuclear Technologies, Technical University of Denmark (DTU Nutech) [6]Nuclear Division, Danish Emergency Management Agency (DEMA) [7]Swedish Radiation Safety Authority (SSM) [8]Radiation and Nuclear Safety Authority (STUK)
ISBN	978-87-7893-520-5
Date	January 2020
Project	NKS-B / SLIM
No. of pages	45
No. of tables	0
No. of illustrations	31
No. of references	52

Abstract
max. 2000 characters

In early October 2017, the International Atomic Energy Agency (IAEA) was informed by Member States that low concentrations of Ru-106 were measured in high-volume air samples in Europe from routine monitoring networks. However, no information was given that an accidental release of Ru-106 had taken place. Such events signify the need for prompt and accurate responses from national radiation protection authorities in such cases. This requires that methodologies, suited for operational use, are developed for spatial and temporal localization of the source of contamination based on available monitoring data.

For operational use, nuclear decision-support systems (DSSs) should be extended with modules handling such monitoring data automatically, e.g. by employing the European Radiological Data Exchange Platform (EURDEP), and conveying selected data to the national meteorological centre accompanied by a request to run an atmospheric dispersion model in inverse mode. The aim would be to determine a geographical area in which to find the potential release point as well as the release period.

In the first year of SLIM (2019), the following results are obtained:

- Two case studies are identified and selected, viz. the European Tracer Experiment (ETEX-1) and the October 2017 case of Ru-106 in Europe.
- Methods for temporal and spatial source localization are developed, implemented and described.
- Deterministic numerical weather prediction (NWP) model data are derived from the European Centre for Medium-Range Weather Forecasts (ECMWF) corresponding to the selected cases.
- Quality-controlled measurement data of ground-level concentration are obtained from filter stations.
- The inverse methods for source localization are applied by using the DERMA, MATCH and SNAP atmospheric dispersion models to both cases.

Key words

nuclear emergency preparedness, atmospheric dispersion model, source localization, concentration measurements